TNO PUBLIC

Princetonlaan 6
3584 CB Utrecht
P.O. Box 80015
3508 TA Utrecht
The Netherlands

www.tno.nl

T +31 88 866 42 56
F +31 88 866 44 75

TNO report 2020 R10437

Workflow to evaluate the risk of mineral scaling in a HT-ATES system and application to a potential site in Middenmeer, The Netherlands

Date	16 April 2020
Author(s)	Hester Dijkstra, Cjestmir de Boer, Jasper Griffioen, Mariëlle Koenen
Number of pages	56 (incl. appendices)
Number of appendices	1
Sponsor	EU GEOTHERMICA - RVO
Project name	HEATSTORE
Project number	TNO: 060.28921

Summary

As part of the GEOTHERMICA project HEATSTORE, a workflow was developed for the assessment of scaling risk in a HT-ATES system by application to a potential site in Middenmeer, The Netherlands, to be operated by ECW. The Middenmeer HT-ATES case is planning to inject hot water from 3 geothermal doublets in summer in a sandstone aquifer at a depth of ~400 m, and to retrieve the heat in winter for heating of greenhouses. The developed workflow consists of a groundwater sampling method for an aquifer which high partial pressures of dissolved methane, an experimental set-up and procedure to characterise the act of carbonate scaling and a numerical modelling approach. The experimental procedure enables the sampling and testing of groundwater from HT-ATES sites under the required pressure to prevent degassing of CH_4 and CO_2, to prevent the occurrence of unwanted geochemical changes of the water. The experimental procedure consists of batch experiments in a pressure vessel, with groundwater sampled at the site. Steel or aquifer sediment can be added to the autoclave to represent conditions in the engineered part of the HT-ATES system or the aquifer, respectively.
The experiments with groundwater sampled from a test well at the potential site in Middenmeer demonstrated that, even though the water will be oversaturated with carbonates such as calcite, dolomite and siderite when it is heated from ambient temperatures to 85°C, precipitation is not predicted to occur within several days unless calcite seeds are present. Calcite seeds added to the autoclave seemed to provide proper growth surfaces for additional Ca and/or Ca-Mg carbonate to precipitate, unlike the steel plate. The addition of sediment from the aquifer, consisting of primarily quartz with minor additions of feldspar, carbonates, clay minerals and foraminifera, did not show signs of mineral precipitation, possibly related to the presence of organic material in the sediments which can prevent or delay carbonate scaling. In an actual HT-ATES system, the residence time of water in the engineered part (wells, pipes, heat exchanger) is in the order of minutes to hours and flow conditions occur. Hence, the batch experimental conditions are much more conservative and the absence of mineral precipitation in the absence of proper nucleation sites suggests that scaling by carbonate minerals is more likely to occur in the calcareous aquifer around the hot well. This hypothesis is based on a limited number of experiments, from which the operational hydrochemical processes could not be well established due to the minor changes especially when compared to the analytical accuracies. Additional experiments and potentially an adaptation in water analysis methodology (1 series for all samples instead of multiple series) are needed to further investigate the risk of scaling and the most likely location of scaling in the HT-ATES system.

Although preliminary, the experiments suggest that the probability of scaling for the potential site in Middenmeer is higher in the aquifer where crystal growth sites for carbonate minerals are present, rather than in the engineered part of the HT-ATES system. A reactive transport model, based on the geology of the site in Middenmeer, was developed to evaluate the processes and impact of scaling in the aquifer upon seasonal loading and unloading by hot water. Although the experiments indicated neither strong calcite precipitation nor strong dolomite precipitation, the simulations based on thermodynamic equilibrium conditions predict that dolomite will precipitate and calcite will dissolve to support dolomite scaling by providing additional calcium. Whether this process is a realistic scenario and at which rate is currently unclear. A

scenario in which only calcite is allowed to react predicts that calcite will precipitate around the hot well. The unloading of the HT-ATES site, with extraction of hot water from the hot well and injection of cooled water in the cold well may result in carbonate dissolution around the cold well. With each annual loading and unloading cycle, the reactions are predicted to continue and progress further into the aquifer, with a continuous decrease of the porosity and permeability around the hot well and increase around the cold well as a result. The extent and impact of the carbonate reactions are subject to uncertainties related to simplifications in the model, but the trends demonstrate the risk of scaling around the hot well and potential clogging of the aquifer when carbonate precipitation occurs rather fast.
The addition of CO_2 to the hot water prior to injection could prevent the formation of scale, but the dosing should be done with care to prevent the dissolution of all carbonates and a corresponding increase in porosity. Porosity increases could be accompanied by geomechanical effects such as pore collapse. In addition, the CO_2 may need to be removed during the unloading phase prior to injection at the cold well to prevent enhanced dissolution of carbonates.

Naturally, these experimental and numerical modelling results are specific for the groundwater composition and experimental/modelling conditions used for this case. The workflow as used in this study, or an adaptation of such a workflow, can be used for a first evaluation of scaling risks in any HT-ATES system. During operations, careful monitoring of the processes, model calibration and timely adaptation of the operational design would be recommended.

Contents

1 Introduction

In a High Temperature – Aquifer Thermal Energy Storage (HT-ATES) system, (excess) heat is temporarily stored, generally to match heat supply and demand on a seasonal base. Groundwater extracted from an aquifer at relatively shallow depths (few hundreds of meters) will be heated via a heat exchanger with the excess heat and subsequently the hot water will be reinjected in the same aquifer using a second, 'hot' well. This is the loading phase of the HT-ATES system. By the time the heat is required, generally in the winter, the hot water will be back-produced from the hot well, the heat will be extracted using the heat exchanger and the cold water is re-injected into the cold well. This is the unloading phase of the system. These loading and unloading phases are to continue on an annual basis.

In the Western part of the Netherlands which is the subject of this research, the groundwater in the aquifer is generally saline and anoxic, and is presumably saturated with respect to carbonates like calcite. Furthermore, the water generally contains dissolved CO_2 and CH_4. During the loading phase, the production of relatively cold water in the production well results in a pressure decrease, with the risk of CO_2 and CH_4 degassing. CO_2 degassing will increase the pH of the water, thereby changing the chemical equilibrium of the system. Then, the temperature of the water is increased in the heat exchanger, which also changes the chemical equilibrium of the water. Both the higher pH and the higher temperature will lower the solubility of carbonate minerals such as calcite, which may cause precipitation of carbonates and the associated risk of carbonate scaling (Eq. 1). For this reason, scaling by carbonate minerals, and primarily calcite, is often considered as a high risk for the operations of a HT-ATES site.

$$CaCO_3(s) + H_2CO_3(aq) \rightleftharpoons Ca^{2+}(aq) + 2HCO_3^-(aq) \qquad \text{(Equation 1)}$$

Scaling may give rise to technical problems with respect to the surface installations (tubes, pumps, well) as well as the filter sand or storage aquifer in close vicinity to the well. However, dissolved PO_4 and dissolved organic carbon (DOC) and also Mg in seawater type water may inhibit the carbonate precipitation process when they are present at sufficiently high concentrations (Griffioen and Appelo, 1993), which is to be expected for groundwater in the Western Netherlands. Hence, there is a need to determine the risk of scaling beforehand with experiments and numerical models in which the process of heat storage is simulated.

The aim of this task was to develop an experimental and modelling workflow for the evaluation of the risk of scaling in a HT-ATES system and the impact of water treatment to mitigate the risk. The workflow is developed by application to a potential HT-ATES system at Middenmeer in The Netherlands, to be operated by network organization and private grid operator ECW (Energie Combinatie Wieringermeer). The experimental workflow involves geochemical batch experiments using groundwater from the test well in Middenmeer, and sandy sediment from the aquifer. The batch experiments will demonstrate whether mineral precipitates can be expected due to heating of the groundwater on the timescales at which the water is present in the engineered part of the system (wells, pipes, heat exchanger) based on thermodynamics and kinetics of scale precipitation. The addition of sandstone material to the batch experiments will show whether the availability of mineral

nucleation sites will enhance the mineral precipitation. If this is the case, the risk of scaling could be larger in the aquifer around the injector than in the engineered part of the system. Subsequently, the results of the experimental study are used to develop a reactive transport model of the aquifer to assess the potential impact of carbonate scaling on the injectivity of the HT-ATES aquifer and the impact of water treatment as a mitigation measure.

The report is constructed as follows:

- Chapter 2 gives a short description of the potential HT-ATES system at Middenmeer and the geological, hydrological, sedimentological and geochemical conditions in the subsurface;
- Chapters 3 and 4 describe the experimental methodology and results, respectively.
- Chapter 5 describes the reactive transport simulations.
- Chapter 6 ends with a discussion and conclusions of the results for HT-ATES in general, and for the potential site in Middenmeer in particular.

2 ECW HT-ATES site in Middenmeer

2.1 Introduction

ECW (Energie Combinatie Wieringermeer), located in Middenmeer at the Agriport A7 project area, has three operating geothermal doublets. These doublets provide 22% of the heat required by the greenhouses in the area (De Jonge, 2017). The geothermal water is transported to ECW's geoplant and from there the heat is distributed to the greenhouses by the district heating network.
Currently ECW intends to apply HT-ATES near one of the greenhouses in order to maximize the efficiency of the geothermal systems (Dinkelman, 2019). After construction of the HT-ATES well the excess heat produced from the Middenmeer geothermal site, will be stored in summer in a HT-ATES system and retrieved in winter. Extracted groundwater will be heated via a heat exchanger with the excess geothermal heat from 15°C to around 85°C and subsequently the water will be reinjected and stored at depths of around 300-350 meters. Currently almost 400 ha of greenhouses is connected to the geothermal heating network. In the future, this could be extended to about 600 ha (De Jonge, 2017). The HT-ATES is planned to be installed in Middenmeer, the approximate coordinates are X = 132.000 and Y = 535.000, and the location is shown in Figure 1.

Figure 1. Location of the HT-ATES at the Tussenweg in Middenmeer, the location of the hot (w) and cold (k) well are highlighted (De Jonge, 2017).

2.2 Hydrogeology

At the site, aquifer layers in the Maassluis Formation (280-420 m-mv) and Oosterhout Formation (420-520 m-mv) were identified as most suitable for HT-ATES (De Jonge, 2017). REGIS (regional geohydrological information system), a digital geological model (DGM) and well descriptions from the MDM-GT-01 and MDM-GT-05

geothermal wells, were used to determine the suitability of the aquifers. This was done by analysing the permeability, thickness and continuity of the formations (De Jonge, 2017).

Figure 2 and Figure 3 show hydrogeological cross-sections of the area and indicate the hydrogeological units present. The Maassluis and Oosterhout Formations are located at a depth of 270-450 relative to NAP and are horizontally layered at regional scale. The Maassluis Formation is part of the Upper North Sea Group and of Early Pleistocene age. It consists of very fine to medium coarse (63-300 µm) (often calcareous) sand. Also present are silty and sandy clay layers and lenses. The thickness of the Maassluis Formation is variable and is controlled by the geometry of the North Sea basin at the time of deposition. The thickness increases towards the North West and between Texel and Vlieland the formation can be up to 250 m thick (Huizer and Weerts, 2003).

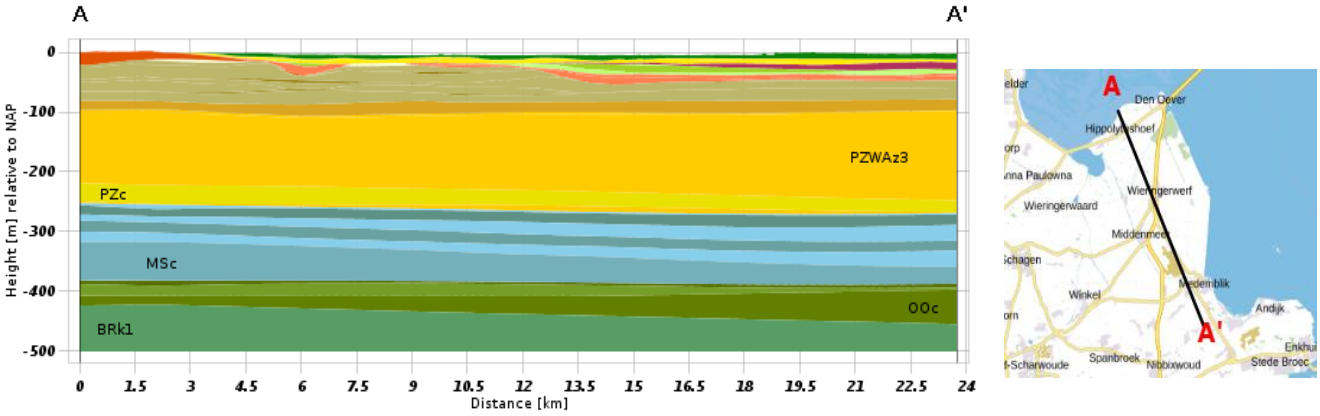

Figure 2. Cross section of the Middenmeer area, from NW to SE. From: REGIS II v.2.2 (2017).

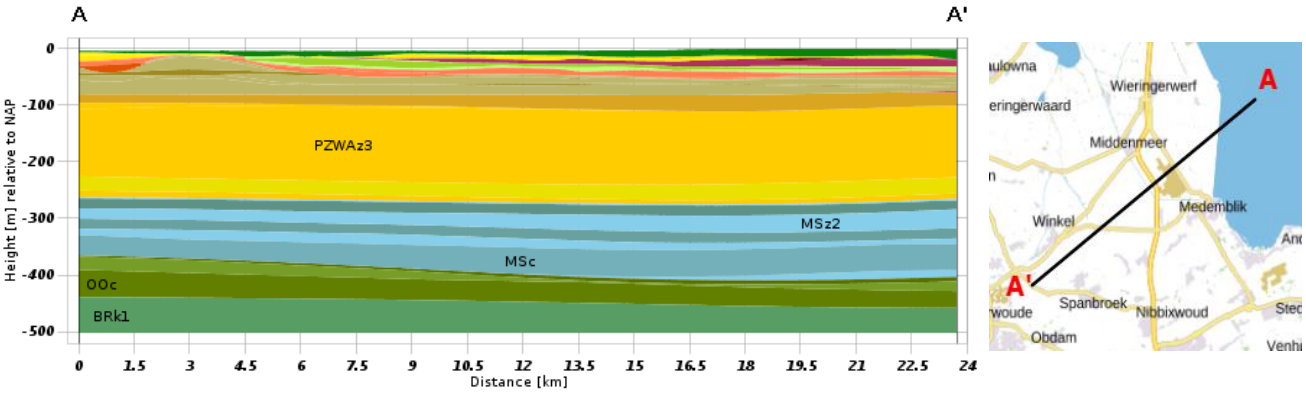

Figure 3. Cross section of the Middenmeer area, from NE to SW. From: REGIS II v.2.2 (2017).

The Oosterhout Formation, which is also part of the Upper North Sea Group, was deposited during the Late Miocene/Pliocene. The formation consists mainly of very fine to medium coarse (105-420 µm) sand with clay layers and lenses. These lenses are often rich in shell fragments. The thickness of the formation varies between 1 - 150 m. The upper part of the Oosterhout Formation (ca 420-460 m-mv) has a

relatively high permeability, the lower part mainly consists of impermeable clays (De Jonge, 2017).

2.3 Evaluation ECW test well

A test well was drilled in March-May (phase 1) and August-September (phase 2) 2019 and reached a depth of 471 m below ground level (IF Technology, 2019). The well crosses five aquifers and in each aquifer an observation location made of PVC was installed. The well was used to evaluate the potential of the two targeted horizons (aquifer 4 and aquifer 5, see Figure 4). The parameters used for the evaluation were the maximum flow rate, risks of mixing of water and gas, gas pressures, reactivity, grainsize distribution and crossflow.

The maximum flow rate was tested for the two target aquifers (Figure 4). For the 4th aquifer the maximum flow rate was determined to be 150 m^3/h and for the 5th aquifer this was lower with 100 m^3/h. The crossflow was determined to be 0.75 m^3/h from the 5th to the 4th aquifer. Production from both aquifers would provide a higher total flow rate but would also require higher construction costs to prevent cross flow. Another possible issue when producing from two aquifers is the risk of mixing of the groundwater and their dissolved gasses from the two layers. A significant amount of methane is present in the 5th aquifer (c. 151 mg/l) with a partial pressure of 13 bar (versus 3 bar in aquifer 4). This high gas pressure would create a more complex system and the presence of methane also creates a safety risk.

With respect to the grainsize distribution in the two aquifers, the 4th aquifer also appears more favourable because of its larger and more homogeneous average grainsize (Figure 5). Aquifer 5 appears to be more heterogeneous which increases the risk of sand production at higher flow rates.

All the findings above combined led to the selection of only aquifer 4 as the most suitable for heat storage. Combining the two aquifers would increase the yield, but the risks and extra costs that would accompany this are greater than the benefits.

Based on these considerations, it was decided by ECW to select the 4th aquifer for HT-ATES at this site.

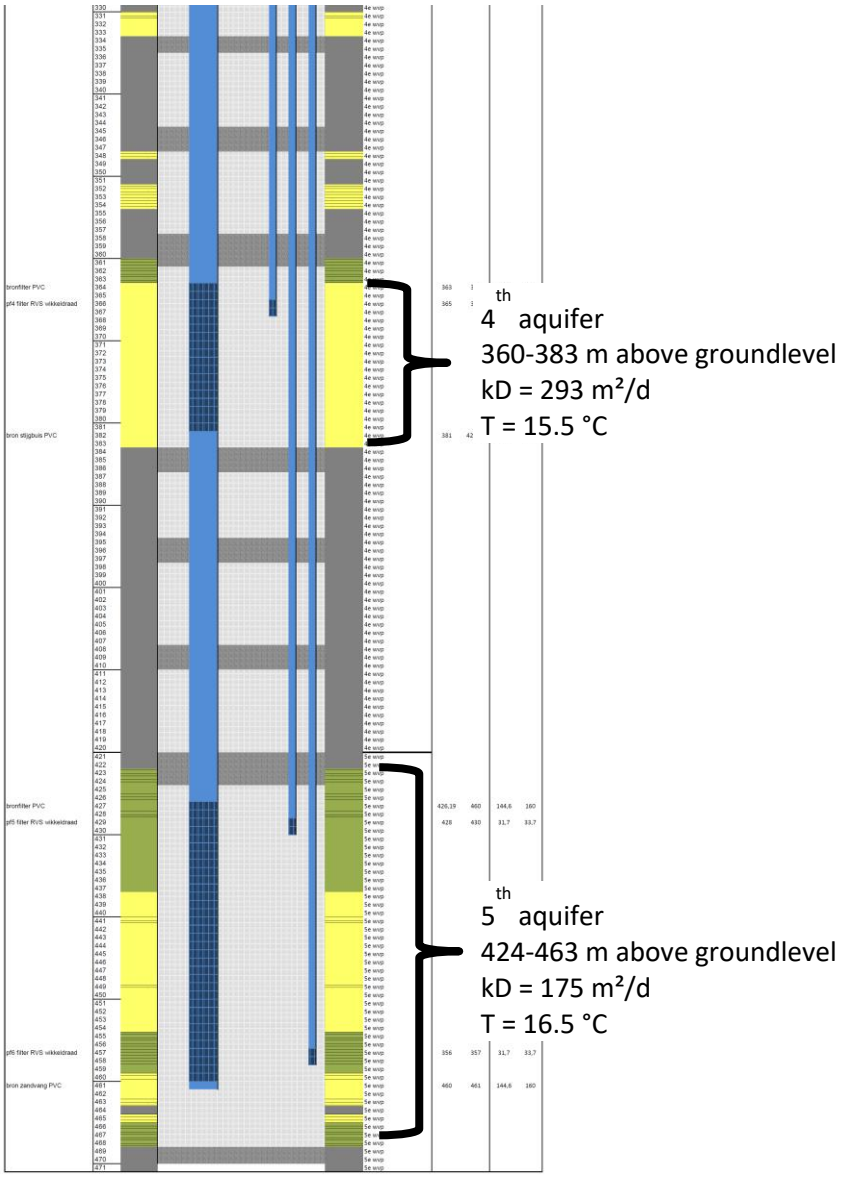

Figure 4. Stratigraphy of the test well showing the two targeted horizons, with their depth, permeability and temperature (WVP = aquifer; IF Technology, 2019).

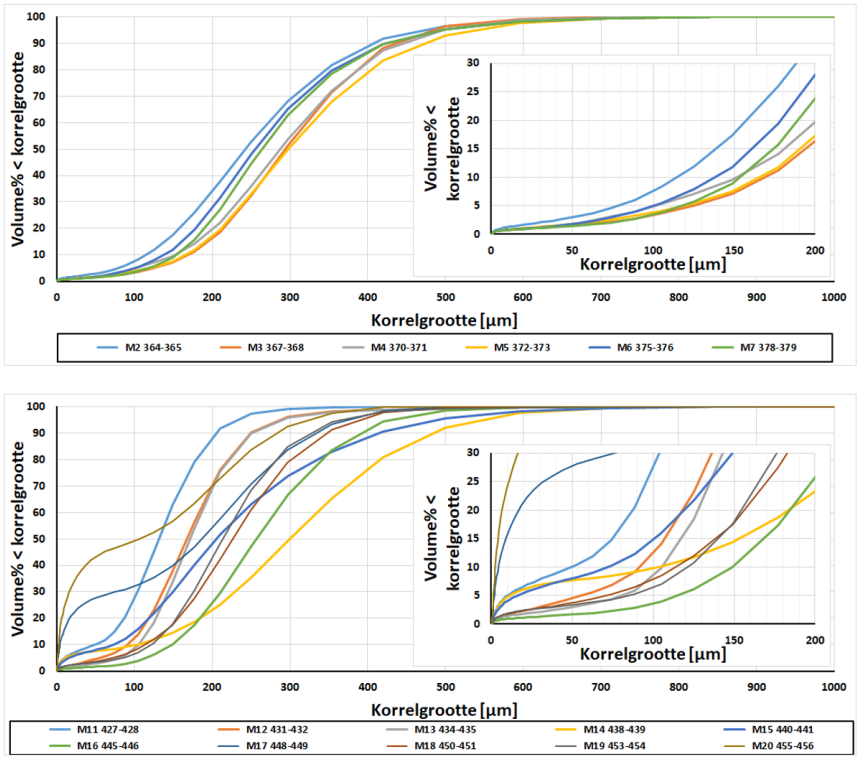

Figure 5. Grainsize distribution of sample from aquifer 4 (top) and aquifer 5 (bottom) (IF Technology, 2019).

3 Experimental methodology

3.1 Groundwater sampling

For the experiments, groundwater samples were collected from the test well in Middenmeer. These samples were collected after the 5th aquifer had been closed off and after the production test for the 4th aquifer had been executed. During the production test the water was pumped from the well for several hours at a rate of 60 m^3/h. This ensured the well to be cleaned and the water samples to only contain representative groundwater from the 4th aquifer.
The hydrostatic pressure in the aquifer is around 30 bar and the conditions are anoxic. This causes all the gasses present in the aquifer to be dissolved in the groundwater. Therefore, the sampling had to be executed under pressure and also in absence of oxygen. PHREEQC was used to calculate the pressure necessary to prevent any degassing of the dissolved CO_2 and CH_4. For the 4th aquifer this requires a pressure of 3.5 bar.

Figure 6. Left: hose used for sampling attached to well head, pressure meter shows 8 bar sampling pressure. Right: bypass installed for pH, oxygen and EC measurements.

The sampling was done using a KeyKeg beer keg which is a plastic keg with an aluminium lined, gastight inner bag which is designed for 4.2 bar continuous use, 7 bar of maximum short term use (including 7 bar factory tested) and is designed for 12 bar failure pressure. The outer container was pressurized with compressed air to 3.5 bar. Subsequently the vessel was attached to the well with a hose and the flow rate was lowered to increase the pressure in the well to around 8 bar (fig. 6). Three KeyKegs (2x 10 liter, 1x 20 liter) were filled with groundwater using this procedure, the pressure in the keg was maintained at 4 bar. Upon sampling, the groundwater had a temperature around 15°C and the KeyKegs were stored in the fridge to maintain low temperatures. This was done to prevent any decomposition of dissolved or suspended organic matter and minimize bacterial activity.

A bypass was attached during sampling in which pH, electric conductivity, temperature and dissolved oxygen were measured (Figure 6). The alkalinity was measured immediately after sampling with a Hach alkalinity test kit. Furthermore water samples were collected for water composition analysis prior to and after the experiments.

3.2 Experimental set-up

The experimental set-up was developed at the high pressure and temperature facility of the material solutions (MaS) department at TNO Eindhoven, The Netherlands. Two stainless steel autoclaves were used for the experiments. Inside these autoclaves two PVC beakers were placed which prevented contact of the groundwater with the stainless steel wall of the autoclave in order to prevent corrosion. Inside this beaker a small stainless steel plate was placed representing the stainless steel perforated section at the bottom hole of the well and (parts of the) surface installations. The autoclave has two outlets, one connected to a dip tube (¼" PTFE tubing) and the other without a dip tube. This allows sampling of either water (dip tube) or headspace (no dip tube)
All experiments performed to investigate scaling during heating of the formation water were conducted with the stainless steel plate present in the autoclave to represent conditions in the engineered facilities (surface facilities and well). Additional experiments were conducted with calcite crystals in the autoclave and with addition of sediment from the 4th aquifer to represent conditions in the aquifer in the near well area.
The autoclave had to be filled without atmospheric contamination. For this purpose, a set-up was developed which would allow the autoclave to be pressurized with nitrogen. The KeyKeg and the autoclave are connected through a hose and closed off with two valves (fig. 7). The autoclave is flushed with nitrogen before the filling hose is attached. Before opening the valves the whole system was pressurized up to 4 bar. When opening the two valves the pressure of the autoclave was slightly lowered, allowing flow from the keg into the autoclave. Once the autoclave was filled, 100 ml of groundwater was extracted from the autoclave to create headspace which is necessary to accommodate expansion of the water when the autoclave is heated and potential degassing from the water.

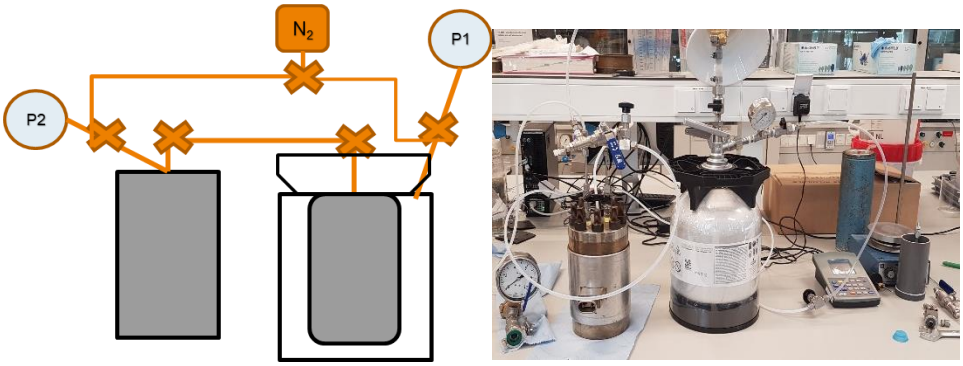

Figure 7. Left: schematic overview of set-up used to transport groundwater from KeyKeg to autoclave. Right: photo of the same set-up.

After filling, the autoclave is closed and placed in a preheated oven for the duration of the experiment. After the experiment the autoclave is taken out of the oven and

the water and headspace was sampled. This is done in a similar way as the filling of the autoclave was done. For the headspace sampling a syringe was attached to the outlet connecting to the headspace of the autoclave and a gas sample was collected from the headspace. With respect to the water sampling, a sampling tube is connected to the outlet with the dip tube, and connected to a 50 ml gas tight Teflon syringe. Before the syringe a bypass for a pH and temperature meter was installed allowing pH and temperature measuring during the sampling (fig. 8). The water was filtered with 0.45 µm syringe filters before entering the syringe.

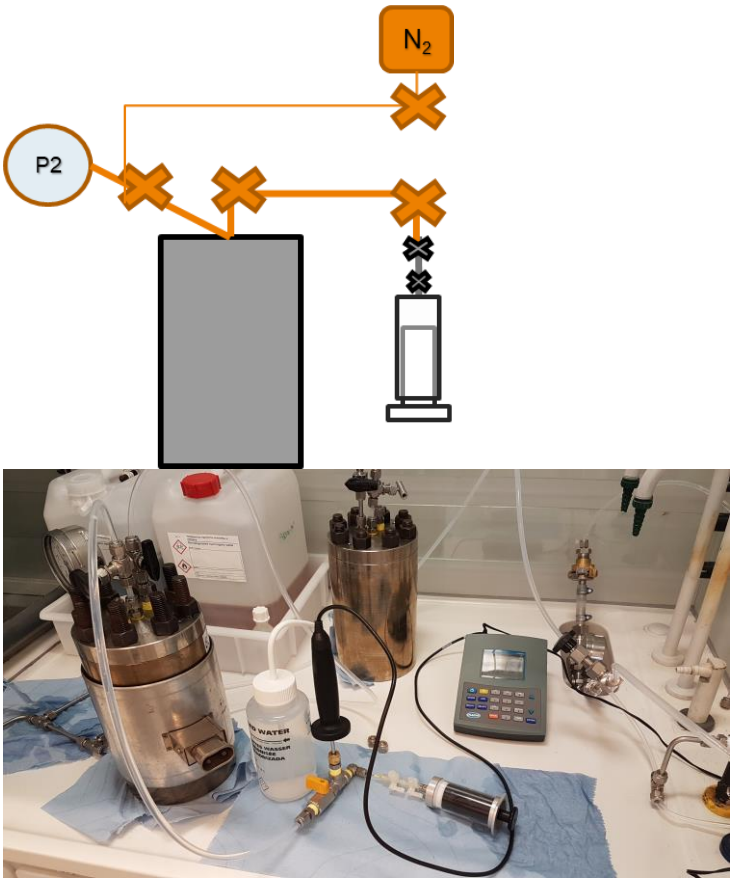

Figure 8. Above: schematic overview of sampling, Below: photo of sampling from autoclave.

3.3 Experimental procedure

The first step was to determine the composition of the groundwater and the gases it contains. The groundwater has a temperature of around 15°C and the total pressure of dissolved gases will be a few bar due to high CH_4 and CO_2 concentrations. All water analyses were executed at the TNO lab in Utrecht and dissolved gases were analysed by Isolab B.V. in Neerijnen, Netherlands.
A series of experiments was performed (Table 1). The first experiment aimed to determine the temperature of the onset of calcite scaling. This was done by heating one autoclave to 50 °C and one autoclave to 80°C.
To ensure reproducibility of the results, experiments 2-5 were all executed in duplicate. Experiment 2 was performed at 85°C with the stainless steel plate in the autoclave. This plate was added, to simulate the stainless steel in the technical simulation which can act as a seed for carbonate precipitation. During this experiment

due to a technical error the alkalinity measurement was not reported. Therefore, experiment 4 was executed to repeat experiment 2. Experiment 3 was also performed at 85°C where calcite crystals were added to the autoclave. The calcite crystals were crushed in an agate mortar and subsequently sieved through two sieves of 0.355 and 0.180 mm. Filtering a fraction with a grainsize between 0.355-0.180 mm. To wash of any dust from grinding and create smooth crystal planes, the crystals were quickly washed in pH 4 diluted acidic acid and rinsed with water afterwards
Experiment 5 was again performed at 85 °C and samples from drilling cuttings were added to the autoclave. Sampling of drilling cuttings is described in paragraph 3.4.

For each experiment a benchmark water sample was collected from the keykeg prior to the start of the experiment. All the water and gas samples were analysed with ICP-MS, GC and IC, additionally the alkalinity was determined with the Hach alkalinity test kit. After each experiment the stainless steel plate, calcite and sediment were analyzed with Scanning Electron Microscope (SEM) and Energy Dispersive X-ray (EDX) in order to investigate potential precipitates.

Table 1. Experimental series with temperature and additions to the autoclave.

Experiment	Temperature	Additions autoclave	Remarks
Experiment 1 MDM501/801	50 / 80 °C	Stainless steel plate	1 autoclave at 50°C, 1 autoclave at 80°C
Experiment 2 MDM802/803	85 °C	Stainless steel plate	In duplicate, alkalinity was not measured
Experiment 3 MDM809/810	85 °C	Stainless steel plate + calcite	In duplicate
Experiment 4 MDM813/814	85 °C	Stainless steel plate	Repetition of experiment 2
Experiment 5 MDM816/817	85 °C	Stainless steel plate + sediment	In duplicate

3.4 Reservoir samples

Cuttings from the interval of the 4th aquifer of the ECW test well were sampled. These cuttings were collected during the drilling of the well and stored in the TNO core library in Zeist, The Netherlands. Cutting samples were collected at 5 meter intervals (Table 2). To be able to analyse the cuttings the bentonite drill mud had to be removed. This was done by washing the cuttings with water and sieving of the sample through a 38 µm sieve to remove the mud fraction from the cuttings. The downside of sieving is that also other clay/silt sized grains might be lost. The cuttings were subsequently microscopically described and analysed with XRD, TGA, SEM and EDX.

Table 2. List of samples collected from the well cuttings. Mbs = meters below surface.

Sample	Depth interval (mbs)
MDM-01	360-361
MDM-02	365-366
MDM-03	370-371
MDM-04	375-376
MDM-05	380-381

4 Experimental results

4.1 Results water composition analyses

4.1.1 Water composition of the ECW test well

Before the start of the experiments, it is important to characterise the composition of the groundwater at the test well. This was done by analysing two groundwater samples. This also gives an indication of the reproducibility of the analyses and of the natural variation. The results are shown in Table 3. In the last column the difference between the two samples is indicated in percentages. Concentrations below the detection limit have been discarded.

Table 3. Groundwater composition of MDM1 and MDM2 samples, collected from the ECW test well. DOC = dissolved organic carbon. Bdl = below detection limit.

Samples ECW test well		**MDM1**	**MDM2**	**Δ MDM1-2**
				%
DOC	mg/L	5.9	5.9	0.5
Chloride	mg/L	10681.1	10760.0	0.7
Nitrate	mg/L	bdl	bdl	n.r.
Sulphate	mg/L	1.4	1.3	-2.5
Aluminium	mg/L	0.026	0.039	50.1
Arenic	mg/L	bdl	bdl	n.r.
Barium	mg/L	0.172	0.172	-0.2
Calcium	mg/L	419.5	420.5	0.2
Cadmium	mg/L	bdl	bdl	n.r.
Chromium	mg/L	0.001	0.001	33.6
Copper	mg/L	0.004	0.002	-62.1
Iron	mg/L	2.4	2.3	-3.2
Potassium	mg/L	95.0	95.8	0.8
Magnesium	mg/L	526.0	519.3	-1.3
Manganese	mg/L	0.2	0.2	-4.1
Sodium	mg/L	5622.0	5726.0	1.8
Nickel	mg/L	bdl	bdl	n.r.
Total phosphorus	mg/L	1.2	1.2	4.4
Lead	mg/L	0.001	0.001	-3.3
Strontium	mg/L	18.7	18.4	-1.3
Zinc	mg/L	0.04	0.04	2.3
Ammonium	mg/L	76.9	77.5	0.9
Ortho-phosphate	mg/L	3.0	3.0	0.5

For the majority of the elements the difference between the two samples is below 5% which is considered as insignificant. For aluminium, chromium and copper the

percentual difference between the two samples is very high. Since the concentrations of these elements are close to the detection limits this is likely a measuring error.

4.1.2 Experiment 1 - Temperature increase (50°C / 80°C)

The duration of experiment 1 was 24 hours. The first autoclave was heated up to 50°C and the second autoclave was heated to 80°C. For each experiment a baseline analysis was done of a water sample collected before the start of the experiment. The results are shown in the Appendix, Table 14.

With respect to the elements important for the scaling process, calcium showed a small increase in both experiments (0.5% and 6.8%). The magnesium concentration decreased (-4.6% and -3.2%), as well as the concentrations of iron (-98.1% and -95.0%) and manganese (-2.9% and -15.7%). The experiment heated to 50 °C shows an increase of dissolved organic carbon (DOC) (115%) The following holds for the minor constituents: albeit at low concentrations, substantial decreases were observed for aluminium (-42%), cadmium (-80%), total-phosphorus (-56%), lead (-73%), zinc (-35%) and ortho-phosphate (-52%), whereas barium (318 %), chromium (32 %), copper (58%) and nickel (560%) show substantial increases.

For the second experiment which was heated to 80 °C, the following elements showed a significant increase: DOC (25%), aluminium (260%), barium (291%), copper (714%), nickel (200%), total-phosphorus (80%), lead (87%), zinc (50%), ortho-phosphate (22%). Overall, both experiments show a strong increase in DOC, barium, copper and nickel.

4.1.3 Experiment 2 - Temperature increase (80-85°C, in duplicate)

The second experiment was executed at 80-85°C, over 5 days. An error was made for vessel MDM802, which was not flushed with nitrogen. Therefore some atmospheric contamination took place which might have influenced the results. Nevertheless, the results of the duplicate experiments show similar trends (Appendix, Table 15).

Calcium showed a small increase in both experiments (2.9% and 5.7%). The magnesium concentration decreased in MDM802 with -2.1% and increased in MDM803 with 0.9%. The concentrations of iron (-50.6% and -49.2%) strongly decreased and the concentration of manganese increased with (11.2% and 21.1%).

Further, the water compositions from both vessels show a strong increase in DOC (277%-127%), sulphate (126%-88%), aluminium (316%-647%), barium (~100%), copper (72%-68%), nickel (1864%-259%) and lead (65%, 313%). A strong decrease was observed for chromium (-23%-8%) and iron (-50%-49%).

4.1.4 Experiment 3 – Addition of calcite crystals (80-85°C, in duplicate)

Experiment 3 was again executed at 80-85°C, but with the addition of calcite seeds. The results are listed in the Appendix, Table 16.

This is the only experiment in which the calcium concentration decreased, even though the decrease is minor (-2.3% and -0.1%). The concentration of magnesium increased slightly with 1.4% in MDM809 and 2.1% in MDM810. The results show a strong increase in DOC for one of the experiments (92%), for both vessels sulphate increased (27-50%) as well as aluminium (139%-69%), arsenic (24-22%), cadmium (46-154%) and nickel (517-158%). For both vessels the concentration of iron (-59-69%), manganese (-22-18%) and ortho-phosphate (-14-19%) decreased. For one of the experiments the concentrations of chromium (-25%) and copper (-31%) decreased. This was not observed in the other autoclave.

4.1.5 Experiment 4 – Repeating experiment 2, Temperature increase (80-85°C, in duplicate)

Because of the atmospheric contamination experiment 2 was repeated. The results are shown in the Appendix, Table 17.

The concentration of calcium and magnesium both slightly increased (1.1% and 0.2% for calcium and 1.7% and 0.5% for magnesium). Manganese showed a small decrease with -1.6% and -1.9%. For the water compositions from both vessels a strong increase in DOC (92%- 57%), aluminium (273%-191%), chromium (17%-46%) and nickel (349%-392%) was observed. The concentrations of iron (-87%-97%) and strontium (-80%-30%) decreased. With respect to arsenic for MDM813 the concentration went up (52%) and for MDMD814 it went down (-19%). For ammonium in MDM813 the concentration went down (-33%) and for MDM14 it increased with 61%.

4.1.6 Experiment 5 – Addition of reservoir material

Experiment 5 was executed at 80-85°C. Sediment from the reservoir was added to the autoclave to investigate the potential impact of nucleation sites. The results are shown in the Appendix, Table 18.

For both vessels the results show a strong increase in DOC (38-43%). A large increase in aluminium (400-794%), arsenic (375-428%) and copper (1136-425%). As well as an increase in calcium (0.5-0.6%), barium (5.6-20%) and strontium (2.2-4.8%). A significant decrease is observed in the concentration of chromium (-20-38%), manganese (-19-11%) and zinc (-87-47%).

4.1.7 General observations and discussion

In all experiments an increase in DOC is measured, this increase varied between 9% and 227%. There is theoretically no reason for DOC to increase, except for the experiment with sediment present, for which it is likely the result of thermally stimulated degradation of solid organic matter from the aquifer sediment (Brons et al., 1991; Bonte et al., 2013). For the rest, although proper care was given to clean the set-up every time, it could be hypothesized that there were small amounts of mechanical oil residues in the valves, o-rings, pipelines or threats of the connectors which were released by the increased temperature or prolonged contact with water. Furthermore, cleaning of the parts and autoclave was done with ethanol and acetone, if the parts did not fully dry this could have been a source of organic carbon in the system.

For the experiments performed without calcite or sediment material added to the autoclave, any increase in elemental concentration is due to either sampling/measurement error or to an side effect caused by e.g. corrosion of the vessel or steel plate, which should therefore also be expected in the ATES installation. The chloride and sodium concentrations do not show large changes, and the changes are not consistent, proving that water evaporation during or after the experiment is not the cause of higher element concentrations.

The minor inorganic components show very large variations. The two baseline sample analyses, performed to evaluate the initial formation water composition in the reservoir and to assess the reproducibility of the analyses, already show large variations. Especially, aluminium, chromium and copper are poorly reproducible but found at low concentrations. For elements present in very low concentrations, the reproducibility is lower than for elements present in larger concentrations. The stainless steel plate consists of, among others, iron, chromium, aluminium, copper

and nickel. Any increase in concentration of these elements could be attributed to corrosion of the plate.
Since Ca carbonate precipitation is the main process of interest, the calcium concentrations are investigated more closely. The measured values for all the experiments are listed in Table 4. All experiments, except the experiments at which calcite seeds were added, show an increase in Ca concentration up to about 25 mg/l. For the two experiments where calcite seeds were added to the autoclave (MDM809 and MDM810), the calcium concentration decreased, even though the decrease is with 0.25 mg/l minor for MDM810.
For the calcium concentrations, the average calcium concentration and the standard deviation was calculated for all the t0 samples prior to the experiments. This aids in determining the significance of the results. The average calcium concentration of these samples was calculated as 418.3 mg/l with a standard deviation of 8.3. The initial compositions were thus equal considering that the samples were analysed in different batches at the laboratory. Only experiments MDM801, 802, 803 and 809 have a change in calcium concentration larger than 8.28 mg/l. A change of 8 mg/l is still small compared to the initial concentration of c. 420 mg/l and analytical accuracy of a few percent. This has to be considered when interpreting the results.

Table 4. Measured calcium concentrations before and after the experiments and the change in concentration for each experiment.

Experiment ID	t0 (mg/l)	t1 (mg/l)	t1-t0 (mg/l)	Δ calcium concentration (%)
MDM501	428.3	430.5	2.3	0.5
MDM801	402.3	429.8	27.6	6.8
MDM802	402.3	413.8	11.5	2.9
MDM803	402.3	425.3	23.0	5.7
MDM809	418.5	409.0	-9.5	-2.3
MDM810	418.5	418.3	-0.3	-0.1
MDM813	414.8	419.3	4.5	1.1
MDM814	414.8	415.5	0.8	0.2
MDM816	424.8	426.3	2.0	0.5
MDM817	424.8	427.0	2.8	0.6

4.1.8 Aqueous speciation

An aqueous speciation calculation was executed using PHREEQC.v3 (Parkhurst and Appelo, 2013) to evaluate the saturation indices for various mineral phases. With PHREEQC.v3 chemical reactions and transport processes can be simulated. As input for PHREEQC the measured water composition data was used including alkalinity and pH as measured on-site (Table 5). The results of the speciation calculation are shown in
The speciation calculation shows that for all samples the saturation index (SI) for calcite and dolomite are positive, which indicates supersaturation. With respect to calcite the SI varies from 0.25 to 1.2. With a maximum SI of 1.2 which was calculated for sample MDM817 (80 °C, with sediment), calcite should precipitate. Since this is not observed, it is likely that the precipitation is inhibited.
For each of the experiments, the SI for calcite after heating is higher than before the start of the experiment, in line with the expectation that calcite solubility decreases with increasing temperature, except for the experiments with calcite seeds (MDM809

and 810). The experiments with added calcite seeds, in which Ca carbonate (re-)crystallisation was observed, have the lowest SI of 0.25, with the SI of the T0 sample being 0.45. This supports the observation of (minor) decrease in Ca concentration and the potential additional Ca carbonate precipitation. The experiments with sediment have a high SI of around 1.1, but the two initial experiments (MDM501 and 801) show a similar result. The high SI values for calcite without the observation of calcite precipitation for all experiments other than the ones with calcite seeds, is probably related to lack of nucleation sites.
The SI values for dolomite are even higher than those for calcite. Similar to calcite, all experiments show an increase in SI compared to their T0 samples except for the experiment with calcite seeds. In the experiment with calcite seeds, small crystals, thought to have precipitated during the experiment, were identified as Ca-Mg carbonate, and might be dolomite. In future experimental work, more EDX analyses, complemented by XRD analyses should be done to confirm this. Rhodochrosite (Mn-carbonate), vivianite (Fe(II) phosphate) and gypsum (Ca sulphate) show negative SIs throughout, which indicates that these minerals will not precipitate.

Table 5. Alkalinity and pH measurements used in the aqueous speciation calculations.

Experiment	**Samples**	**T (°C)**	**Alkalinity (as mg $CaCO_3$/l)**	**pH**
Site sample	MDM1	15.7	291	7.37
Site sample	MDM2	15.7	291	7.37
Experiment 1	MDM500	20 (t0)	300	7.29
Experiment 1	MDM800	20 (t0)	302	7.31
Experiment 1	MDM501	50	286	7.5
Experiment 1	MDM801	80	268	7.4
Experiment 3 (calcite)	MDM009	20 (t0)	280	7.3
Experiment 3 (calcite)	MDM809	80	244	6.8
Experiment 3 (calcite)	MDM810	80	244	6.8
Experiment 4	MDM012	20 (t0)	288	7.2
Experiment 4	MDM813	80	345	7
Experiment 4	MDM814	80	282	7
Experiment 5 (sediment)	MDM015	20 (t0)	330	7.4
Experiment 5 (sediment)	MDM816	80	353	7.24
Experiment 5 (sediment)	MDM817	80	482	7.24

Table 6. Results of the aqueous speciation calculations.

Sample ID	pH	T (°C)	Alk. (eq/kg_w)	si_CO2(g)	si_Calcite	si_Dolomite	si_Siderite	si_Rhodo-chrosite	si_Vivia-nite	si_Gypsum
Site samples										
MDM1	7.3	15.8	0.0059	-1.99	0.33	1.02	0.25	-0.65	-0.25	-3.63
MDM2	7.3	15.8	0.0059	-1.98	0.34	1.02	0.23	-0.65	-1.86	-3.65
T1 samples										
MDM501	7.5	50	0.0058	-2.00	0.94	2.51		-0.17		-3.31
MDM801	7.5	80	0.0055	-1.86	1.17	2.87		-0.15		
MDM809	6.8	80	0.0050	-1.35	0.25	1.06	-1.11	-1.00	-0.79	-3.08
MDM810	6.8	80	0.0050	-1.35	0.26	1.07	-1.42	-1.00	-1.70	-3.07
MDM813	7	80	0.0070	-1.33	0.68	1.89	-1.03	-0.61	-1.38	-3.08
MDM814	7	80	0.0057	-1.48	0.53	1.60	-1.16	-0.74	-1.30	-3.07
MDM816	7.24	80	0.0072	-1.44	1.06	2.67	-0.72	-0.26	-5.80	-3.15
MDM817	7.24	80	0.0098	-1.31	1.20	2.93	0.44	-0.15	-2.71	-3.19
T0 samples										
MDM500	7.29	20	0.0061	-1.94	0.40	1.23	-0.03	-0.59	-1.53	
MDM800	7.31	20	0.0061	-1.96	0.40	1.24	-0.14	-0.57	-3.19	-3.44
MDM009	7.3	20	0.0067	-1.91	0.45	1.32	-0.54	-0.54	-4.15	
MDM012	7.2	20	0.0057	-2.07	0.08	0.56	-0.73	-0.88	0.92	-3.06
MDM015	7.4	20	0.0058	-2.28	0.26	0.94	-0.64	-0.69	1.06	

The potential amount of Ca carbonate precipitation upon heating was investigated by additional PHREEQC calculations. The relevant question is how much carbonate would precipitate down to thermodynamic equilibrium for the experimental solutions? Four scenarios were considered that mimic the technical installation and the storage aquifer conditions:

1 Precipitation of both calcite and dolomite where both minerals are present, i.e, thermodynamic equilibrium for both carbonates and dissolution as well as precipitation possible. This mimics the calcareous storage aquifer.
2 Precipitation of only calcite present with calcite initially present. This also mimics the calcareous storage aquifer where dolomite precipitation is too slow to play a relevant role.
3 Precipitation of both calcite and dolomite where both minerals are initially absent, i.e, only precipitation down to thermodynamic equilibrium possible. This mimics the technical installation that is initially free of carbonates.
4 Precipitation of only calcite where calcite is initially absent, i.e, only precipitation possible of calcite down to thermodynamic equilibrium possible. This mimics the technical installation where dolomite precipitation is too slow to play a relevant role.

Table 7. The potential amount of carbonate precipitation (+) or dissolution (-) down to thermodynamic equilibrium (in mmol/kg water) for four scenarios for four solutions sampled at the end of the incubation experiments. Cc = calcite, do = dolomite.

Scenario	**1. calcite and dolomite both present**		**2. calcite present**	**3. calcite and dolomite may precipitate**		**4. only calcite may precipitate**
Mineral	***cc***	***do***	***cc***	***cc***	***do***	***cc***
Sample						
MDM501	-22.5	11.9	0.86	0	0.63	0.86
MDM809	-19.7	10.3	0.56	0	0.48	0.56
MDM813	-19.1	10.5	1.29	0	0.88	1.29
MDM816	-19.2	10.6	1.58	0	1.01	1.58

Table 7 presents the results for 4 experimental solutions where one should note that 1 mole of dolomite is based on 2 moles of CO_3 (i.e., $CaMg(CO_3)_2$) whereas this is 1 for calcite. When no carbonates are initially present, they can only precipitate from solution and the order of magnitude is around 1 mmol/kg of water. This implies several tens of mg/l for either Ca (scenario 4) or both Mg and Ca (scenario 3). When both minerals are present (scenario 1), a transfer from calcite to dolomite happens as dolomite is thermodynamically more stable than calcite in addition to precipitation from solution. The transfer is now an order of magnitude higher. The next chapter elaborates on this within the context of ATES storage cycles. When only calcite is involved, it is irrelevant whether or not calcite is initially present for the thermodynamic outcome: its presence may influence the kinetics of precipitation from a supersaturated solution but not the equilibrium state.

4.1.9 Quality water composition analyses

Another uncertainty is the quality of the water analyses, which is difficult to validate due to compositional variation in the samples. The alkalinity measurements show a large variation (268-482 mg HCO_3/l) (Table 5). Therefore, it is useful to check the charge balance of the water composition. PHREEQC calculated the electrical balance and the percentage error in the electroneutrality condition for each sample. The results are shown in Table 8. The percentage error lies between 0.5 and 2.4%. This low error shows that the samples are charge balanced. The electrical balance shows values around 0.01 eq/l. The sum of ions is majorly controlled by Na and Cl as major ions from seawater origin. The charge balance is thus satisfactory but it does not provide insight in the analytical accuracy of ions having substantially smaller concentrations. However, the good results for Na and Cl indicate that the quality of the analyses can be trusted.

Table 8. Charge balance and percentage error in electroneutrality condition from brine speciation.

Experiment	Samples	T (°C)	Electrical balance (eq/l)	electroneutrality (% error)
Site sample	MDM1	15.7	0.005	0.74
Site sample	MDM2	15.7	0.007	1.03
Experiment 1	MDM500	20 (t0)	0.009	1.45
Experiment 1	MDM800	20 (t0)	0.009	1.33
Experiment 1	MDM501	50	-0.008	-1.26
Experiment 1	MDM801	80-85	-0.005	-0.8
Experiment 3 (calcite)	MDM009	20 (t0)	-0.006	-1.02
Experiment 3 (calcite)	MDM809	80-85	-0.004	-0.68
Experiment 3 (calcite)	MDM810	80-85	-0.003	-0.5
Experiment 4	MDM012	20 (t0)	-0.009	-1.47
Experiment 4	MDM813	80-85	-0.010	-1.63
Experiment 4	MDM814	80-85	-0.010	-1.56
Experiment 5 (sediment)	MDM015	20 (t0)	-0.008	-1.2
Experiment 5 (sediment)	MDM816	80-85	-0.009	-1.36
Experiment 5 (sediment)	MDM817	80-85	-0.015	-2.38

4.2 Results mineralogical analyses

In order to determine if mineral precipitation occurred during the experiments, the stainless steel plate that was added to the autoclave was analysed with SEM and EDX. After each experiment, the stainless steel plate was shortly rinsed with demi-water and ethanol. This was done to wash of any remaining water and prevent solid deposition of the aqueous species upon drying. Before flushing the plate was visually inspected for precipitates in order to prevent any material from being flushed away.
For the experiment in which calcite or sediment was added to the autoclave, the calcite crystals and sediment grains were analysed before and after the experiments using light microscopy, SEM and EDX. In Section 4.2.1 the sedimentological and mineralogical analyses of the Maassluis sediments are reported. In the subsequent sections, the results from the experiments are discussed.

4.2.1 Characterisation of the 4th aquifer of the Maassluis reservoir

The storage reservoir in the ECW test well is the 4th aquifer in the Maassluis formation. Five samples from drilling cuttings from the storage aquifer were collected and analysed by microscope, SEM/EDX, TGA and XRD (Table 9).

Table 9. Sample list of cutting samples. Mbs = meters below surface.

Sample	Depth interval (mbs)
MDM-01	360-361
MDM-02	365-366
MDM-03	370-371
MDM-04	375-376
MDM-05	380-381

All 5 samples were analysed on their mineralogical composition by XRD analyses. The results are shown in Table 10. All samples consist mainly of quartz (81.3-91.4%)

with minor amounts of alkali feldspar (3.8-4.9%) and plagioclase (2.0-4.3%). All samples contain calcite, aragonite and dolomite below < 1% with the exception of sample MDM01 which contains higher amounts of carbonates with 3.5% calcite and 2.6% aragonite. The samples contain minor amounts of titanium oxides (<0.1%). Two samples contain traces of pyrite (MDM01, MDM05). All samples contain layer silicates (1.0-1.7%), chlorite (0.3-0.5%) and kaolinite (0.3-0.5%).

Table 10. Results of mineralogical XRD analysis (in wt-%) performed on samples from the ECW test well.

Mineral	Formula	MDM-01	MDM-02	MDM-03	MDM-04	MDM-05
Quartz	SiO_2	81.3	90.3	91.4	90.9	88.5
Alkali feldspar	$(K,Na)AlSi_3O_8$	4.9	3.8	3.8	3.8	4.6
Plagioclase	$(Na,Ca)AlSi_3O_8$	4.3	2.3	2.0	2.2	3.1
Calcite	$CaCO_3$	3.5	0.8	0.5	0.7	0.4
Aragonite	$CaCO_3$	2.6	0.3	0.1	0.1	0.1
Dolomite/Ankerite	$Ca(Mg,Fe,Mn)(CO_3)_2$	0.3	0.2	0.2	0.1	0.2
Anatase	TiO_2	0.2	0.1	0.1	0.1	0.1
Rutile	TiO_2	0.1	0.1	0.1	0.1	0.1
Pyrite	FeS_2	0.1	n.d.	n.d.	n.d.	0.1
2:1 layer silicates	$K(Al,Mg,Fe)_2(Si, Al)_4O_{10}(OH)_2,(H_2O)$	1.7	1.1	1.0	1.2	1.7
Chlorite	$(Fe,Mg)_5AlO_{10}(OH)_8$	0.5	0.5	0.3	0.3	0.5
Kaolinite	$Al_2Si_2O_5(OH)_4$	0.4	0.4	0.4	0.3	0.5

The large content of quartz in the samples is also visible under the light microscope. The grain size varies from 60 to 300 µm and from poorly sorted (MDM05) to medium to well sorted (MDM01-MDM04). In all samples, shell fragments, mica minerals and foraminifera were observed (Figure 7). Also minor amounts of glauconite and detrital organic material have been observed.
The sampled interval of the reservoir is a coastal marine sand deposit which becomes more fine grained and poorly sorted towards the top and bottom of the interval.
MDM03 sample was added to the autoclave in Experiment 5. Therefore a sample of this interval was also analyzed by SEM and EDX prior to the experiment. Again the large amount of quartz grains is well visible. The light grey coloured grains in Figure 8 contain heavier elements such as titanium and are most likely the titanium oxides that were identified by the XRD analyses. Figure 9 and Figure 10 show various SEM images and EDX point analysis of several grains in the sample other than quartz. Figure 9A shows a grain which contains silica, iron, magnesium and aluminium and some traces of potassium and calcium. Figure 9B is very well rounded detrital grain of titanium oxide (rutile or anatase), due to its weathered surface it is hard to determine which mineral of the two this is. Figure 9C shows a shell fragment, with a spectrum showing the calcium peak indicative of calcium carbonate. Figure 9D is an alkali felspar, containing aluminium, potassium and silica. Figure 10 shows a shell covered with small crystals. The shell consists of calcium carbonate and the crystals consist of iron, magnesium and calcium and are possibly an Fe,Mg,Ca-carbonate such as Fe-dolomite or siderite on top of Mg-calcite.
A thermogravimetric analysis (TGA) was performed on the five samples. During TGA, the samples are continuously heated up to a final temperature of 1000°C and the weight loss for a certain temperature interval is then indicative for a specific component in the sample, for example as CO_2 from Ca carbonate. Around 2-3 grams

of sample material was used and the weight loss as a result of heating was measured continuously during the process.
Up to a temperature of 450 °C, the weight loss is caused by the oxidation of organic material from the samples. From 450-550 °C the weight loss is due to a number of different components, such as dehydration of clay minerals or more recalcitrant organic material. From 550-825 °C the losses are caused by the decomposition of carbonates. Losses at higher temperatures are unclear for Dutch sediments. The results are shown in Figure 11. Sample MDM01 shows a different pattern than the other samples. Whereas MDM01 shows a more or less flat line up to 600 °C the other samples show a gradual weight loss up to 600 °C. This implies a lower amount of organic material and clays and a larger amount of carbonates present in sample MDM01 compared to the other samples. This is consistent with the XRD results. At a temperature above 600 °C all samples show a steep drop in weight. Above 700 °C the line becomes more or less horizontal, at which point only the silicates are left. The total weight losses are small even for MDM-01. The sediments analysed are thus low in organic matter, clay and/or carbonates.

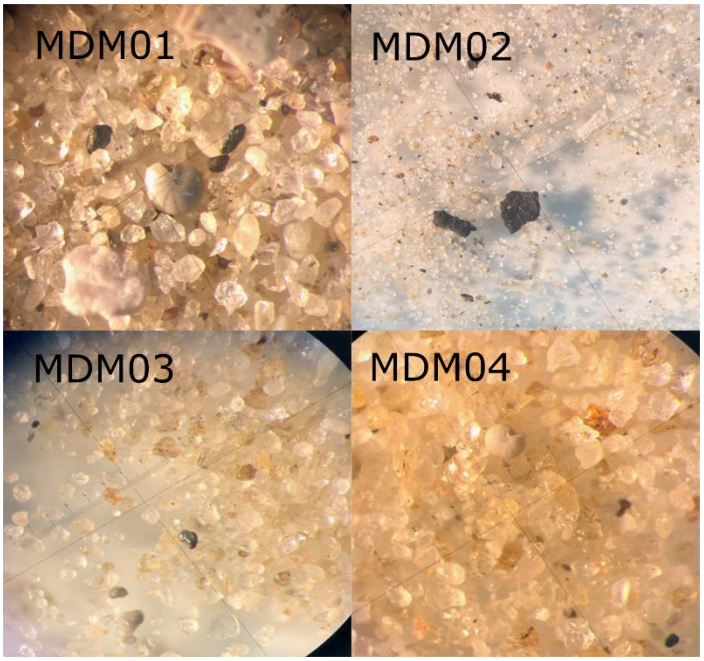

Figure 7. Light microscopy images of MDM samples.

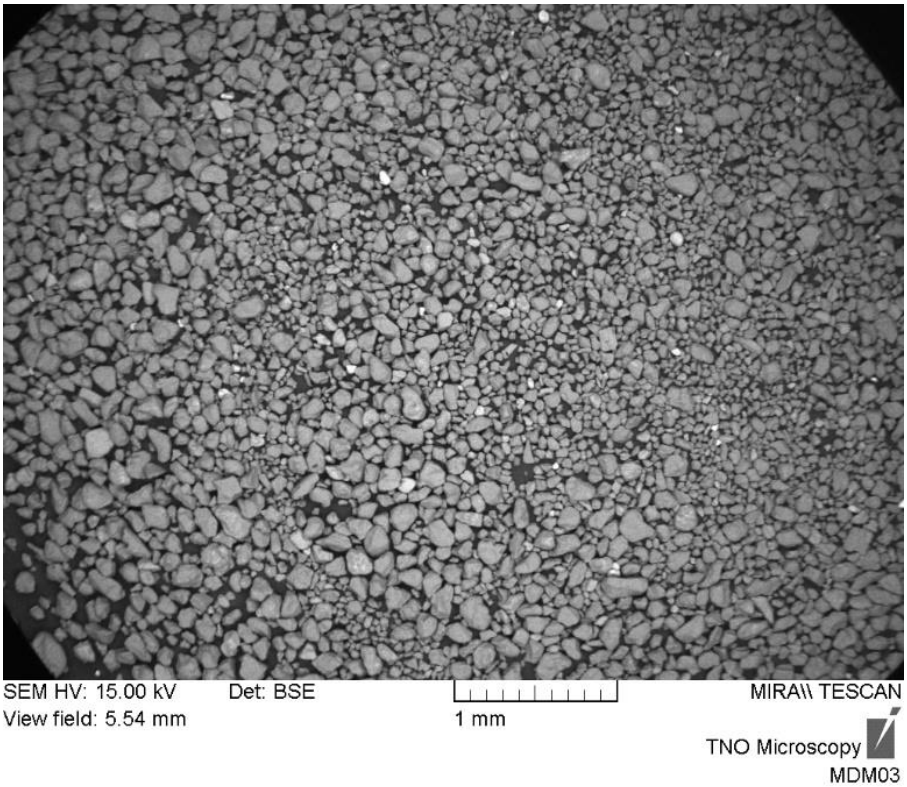

Figure 8. SEM image giving an overview of the MDM03 sample before the experiment.

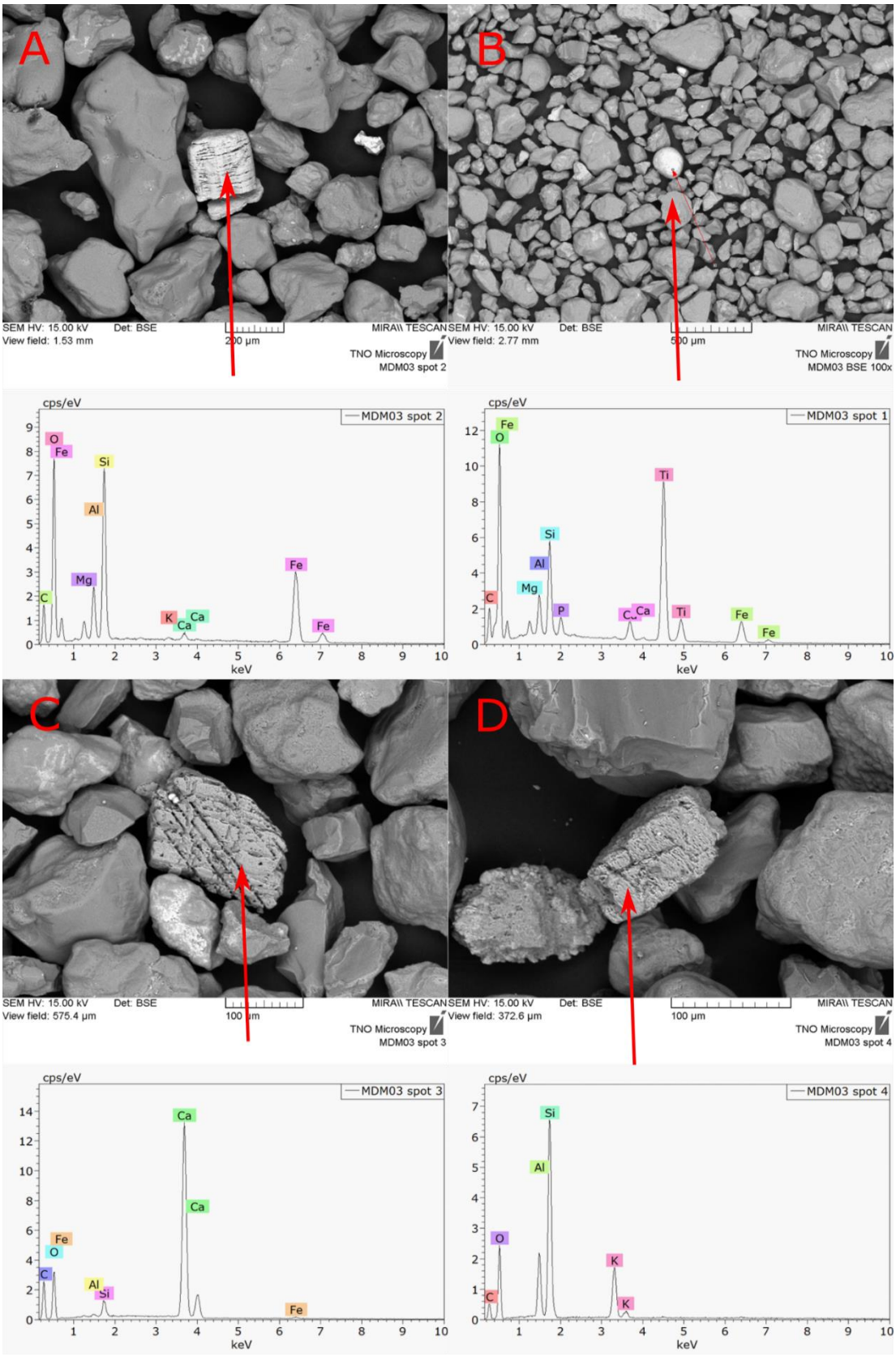

Figure 9. SEM and EDX analyses of MDM03 sample.

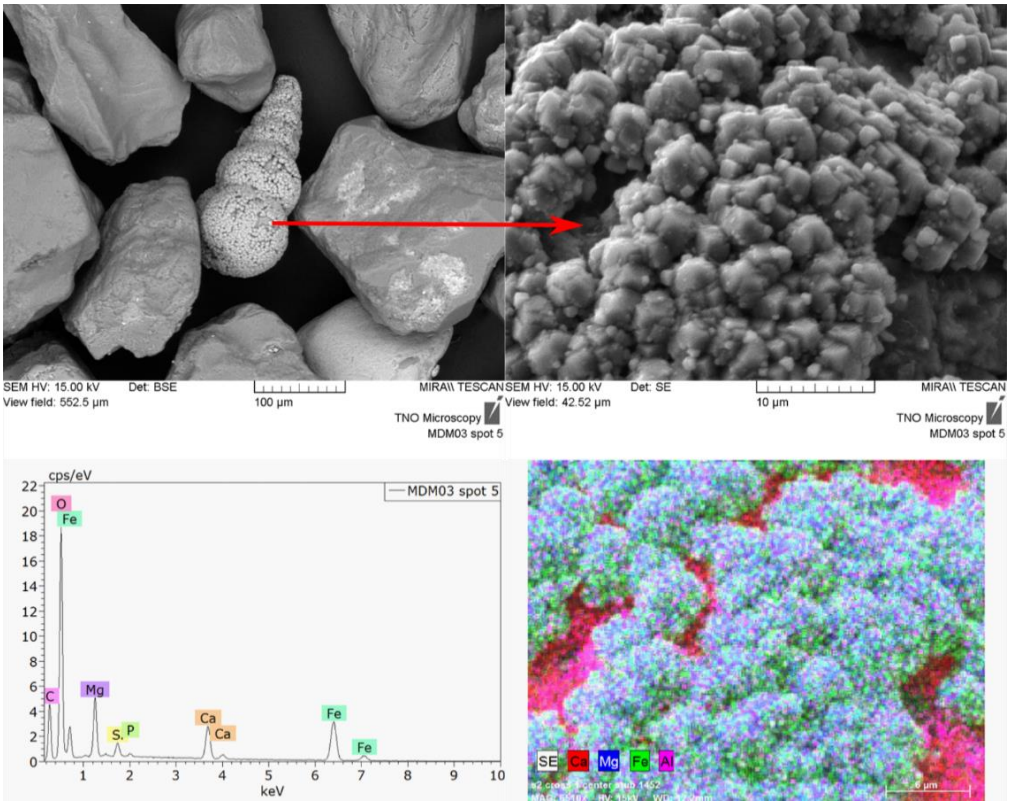

Figure 10. SEM and EDX analyses of sample MDM03.

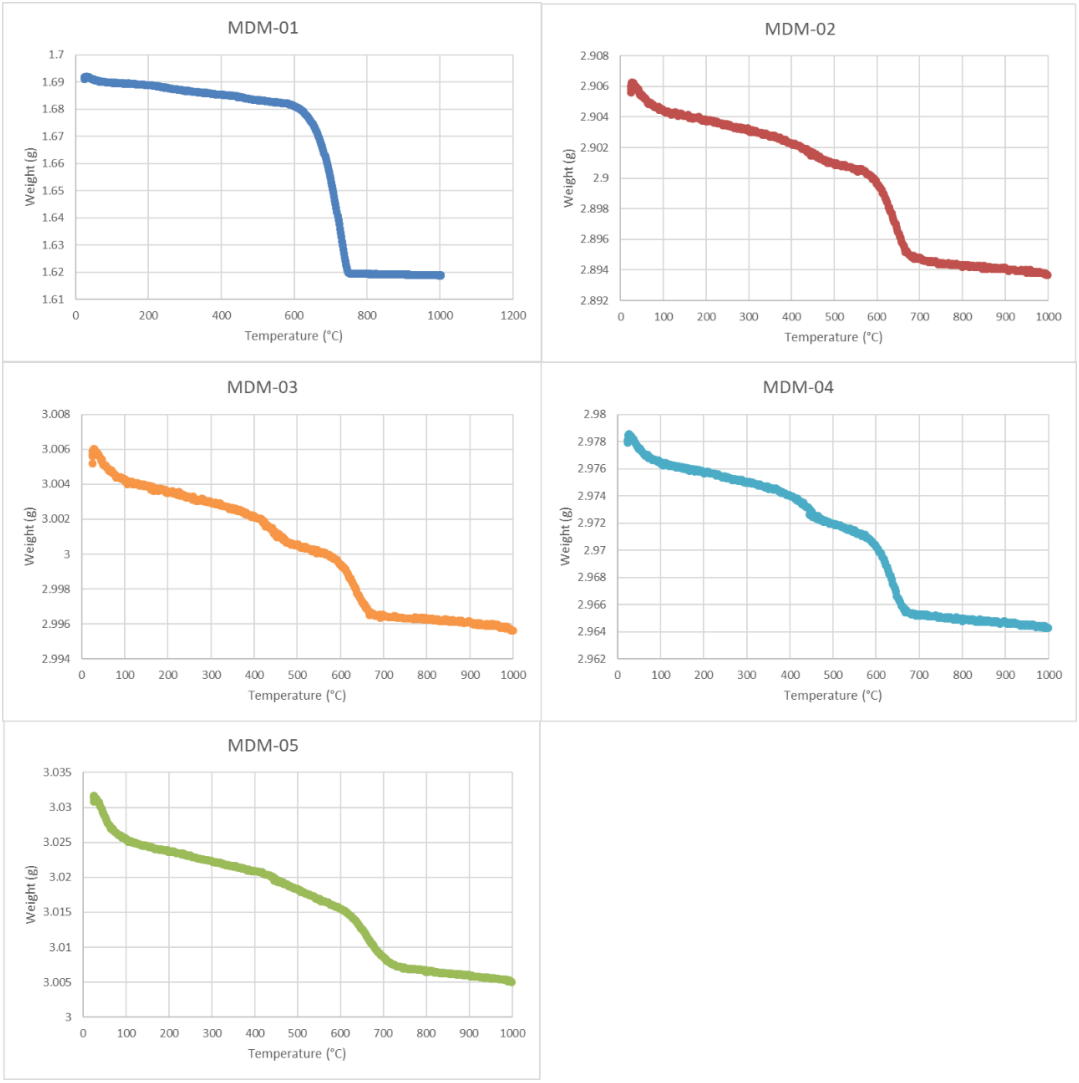

Figure 11. Results of TGA analyses, weight of the sample on the y-axis and temperature on the x-axis.

4.2.2 *Experiment 1, 2, 4 – stainless steel plate, 80-85 °C*

Experiments 1, 2 and 4 were executed with only the stainless steel plate present in the autoclave in addition to the groundwater. For experiment 1, one autoclave was heated to 50°C and one autoclave was heated to 80-85°C, over 24 hours. In experiments 2 and 4 both autoclaves were heated to 80-85°C for a duration of 6 days. Figure 12 shows the SEM images of stainless steel plates from the experiments. The stainless steel plate had a rough and a smooth surface. In the SEM the smooth surface can be seen in Figure 12A, E, F and the rough surface is observed in Figure 12B,C, D as having an elephant skin-like texture.

Although the stainless steel plates were rinsed prior to analysis, some halite crystals did precipitate and show up in all SEM images (Figure 12A-F) as the cubic crystals that have precipitated on the surface of the stainless steel. Figure 12C shows some amorphous precipitates for which any crystalline structure seems to be lacking. EDX analyses showed that these precipitates consist of a wide variety of elements, suggesting that these are most likely the result of the drying of remaining water drops on the surface of the plate after opening of the vessel.

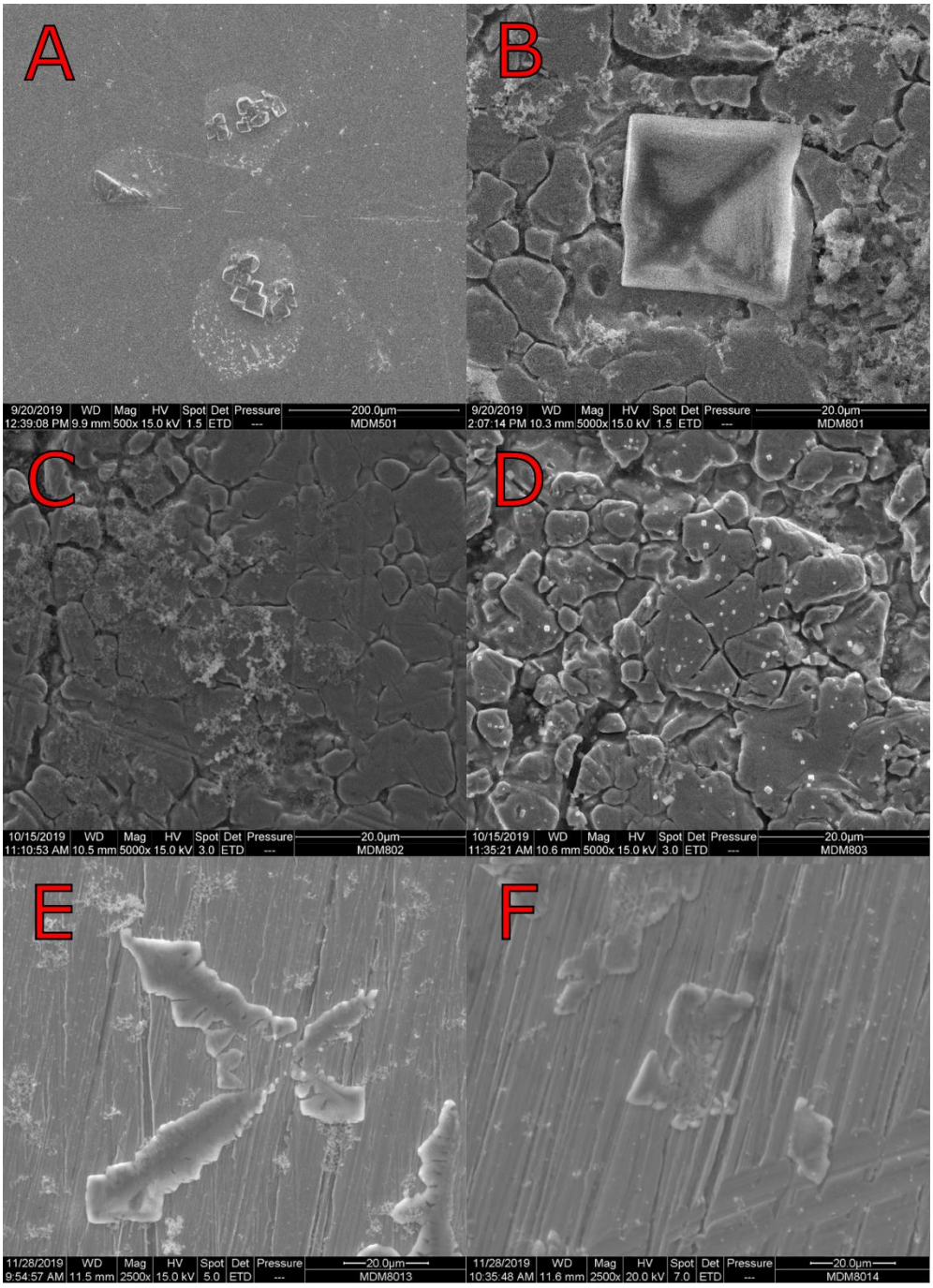

Figure 12. SEM images of the stainless steel plate after the experiments.

4.2.3 Experiment 3 – calcite + stainless steel plate, 80-85 °C

In experiment 3, Ca carbonate seeds were added to the autoclave in addition to the stainless steel plate. Prior to the experiment, the calcite seeds consisted of very distinct crystals with a grainsize between 0.355-0.180 mm (Figure 13). After the experiment the calcite crystals appeared to be glued (cemented) together but they were not attached to the stainless steel. Also when comparing the two photos in Figure 13, which are at the same scale, the crystals in the right photo appear to be slightly larger. A recrystallisation seemed to have happened which is unexpected but not impossible as precipitation and dissolution are on-going processes even when there is equilibrium for a mineral.

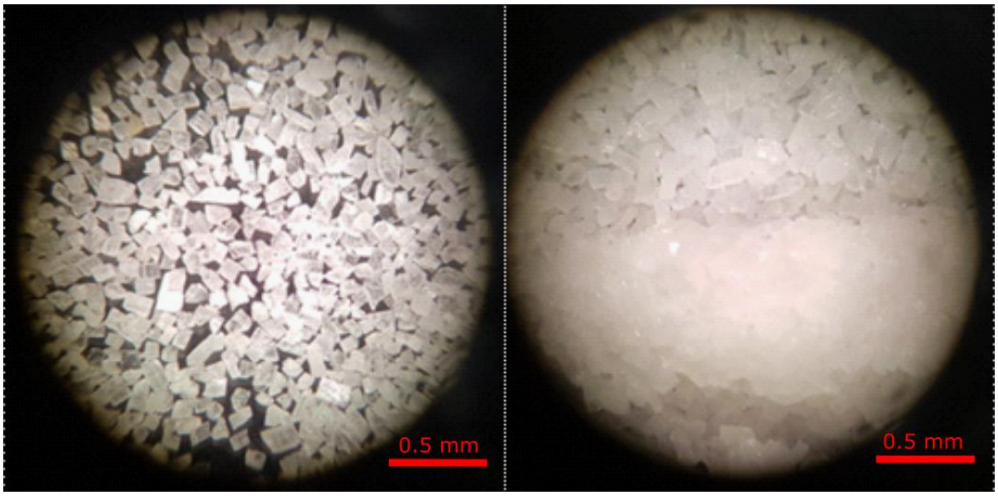

Figure 13. Light microscopy images of the calcite crystals before experiment (left), and after the experiment (right).

Figure 14A-G show various SEM images taken after the experiment. Figure 14A is an image of the stainless steel plate with some small crystals on the surface. Figure 15 is the point analysis spectrum that was taken by EDX from these crystals which show that the crystals are carbonate consisting of calcium and magnesium. The minor elements showing in the spectrum (Cr, Fe, Ni) are artefacts of the stainless steel. These Ca-Mg carbonate crystals are much smaller than the crystals that were initially added to the autoclave (20 µm vs. 180 µm), suggesting that these crystals precipitated during the experiment. For comparison, Figure 14B shows one of the calcite crystals that was initially added.

Figure 14C-G show images of the cemented calcite crystals. At some contact points the individual crystal planes are still very well distinguished (Figure 14D-E) and no clear cement can be observed. However, in the red circles in Figure 14C,E,F and Figure 14G it is very clear that the crystals have been cemented together, making the individual crystals harder to distinguish.

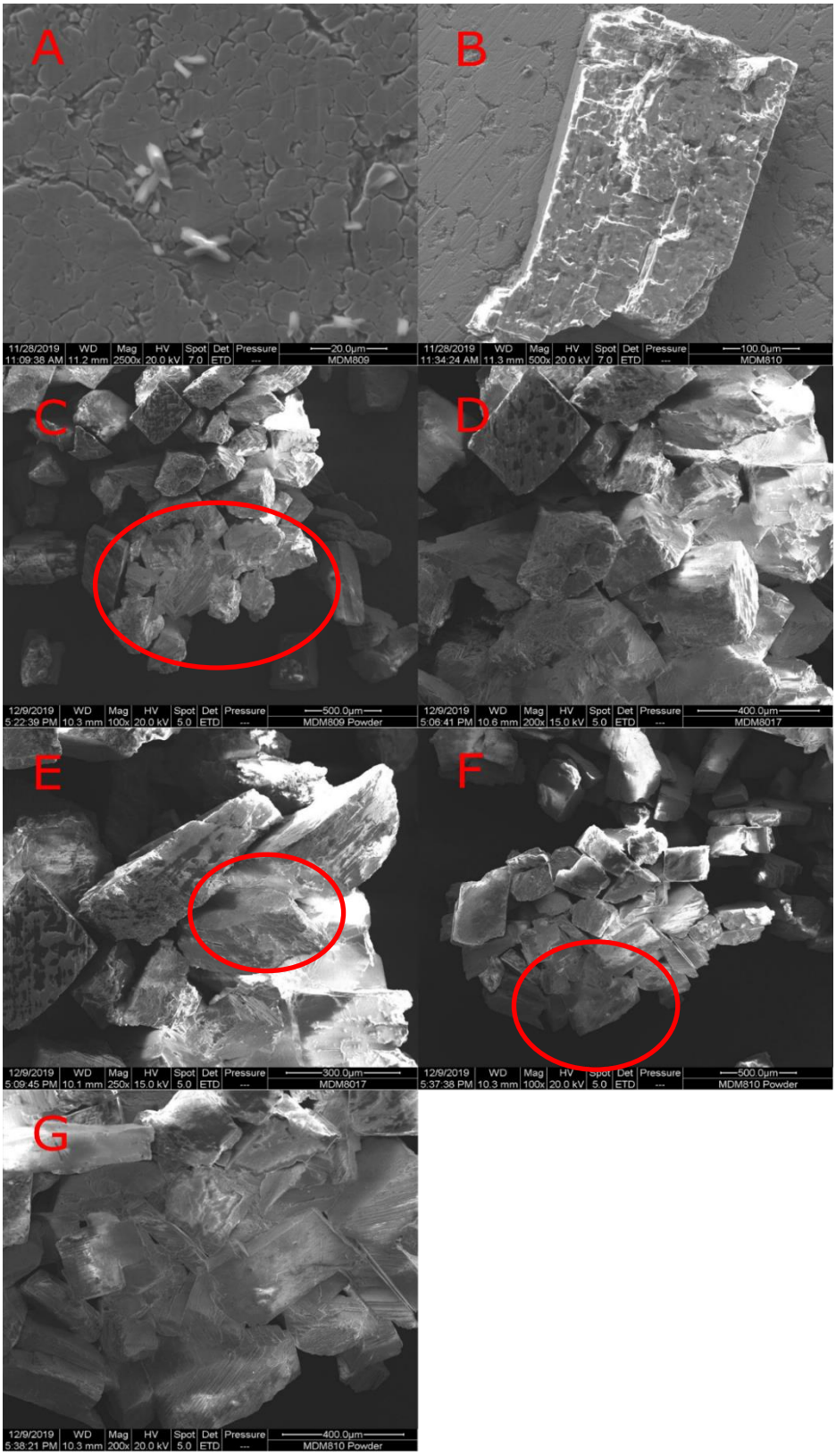

Figure 14. SEM images of experiment MDM809-810 with calcite crystals. Figures A and B show images of the stainless steel plate, C-G show images of the cemented crystals.

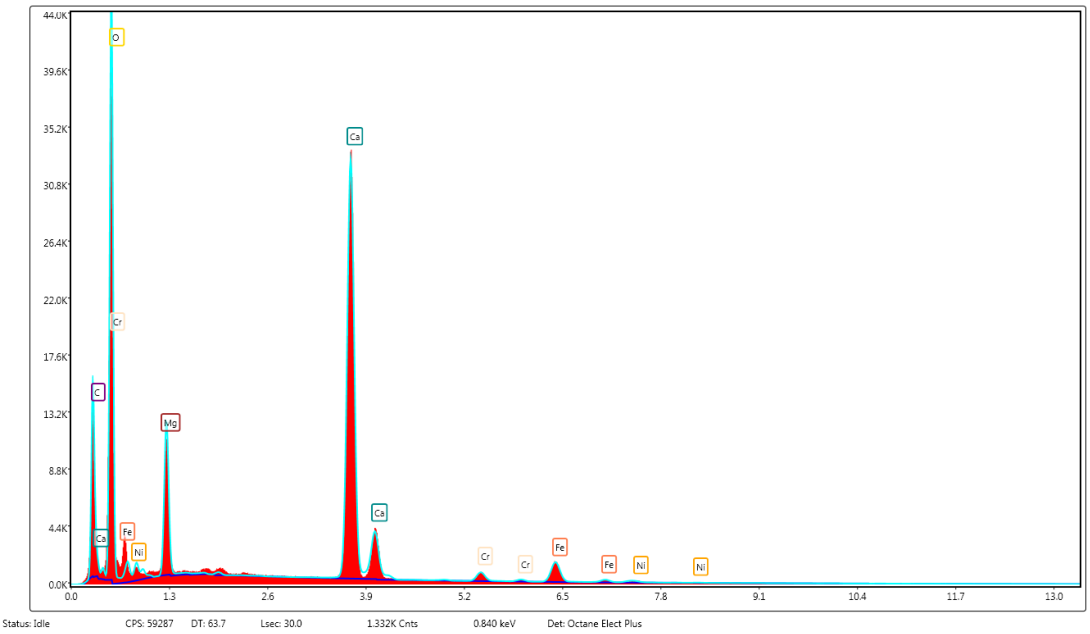

Figure 15. Spectrum from crystals in Figure 14A.

4.2.4 *Experiment 5 – Sediment + stainless steel plate, 80°-85C*

In experiment 5, sediment from drilling cuttings from the ECW test well were added to the autoclave. It was chosen to add a sub-sample from the MDM-03 sample. After the experiment the sediment was collected from the autoclave, quickly rinsed and dried. Figure 16 shows a SEM image with EDX point analysis spectrum on a fine grained precipitate at the stainless steel plate. The image shows an amorphous precipitate containing many elements. The iron and chromium peaks suggest that the signal is mainly derived from the stainless steel plate. The amorphous material is most likely a remnant of a drop of saline water.

Figure 17 shows a series of images, the top left is an overview of the sediment sample from experiment MDM8016. Figure 17 to Figure 19 show images of shell fragments covered with small crystals rich in iron, magnesium with or without aluminium, similar to those observed in the original sediment. The iron, magnesium and aluminium appear to be on the surface and the calcium below it. No changes could be detected with respect to the original material. In Figure 19 the size of the grains is much larger than in the other two figures.

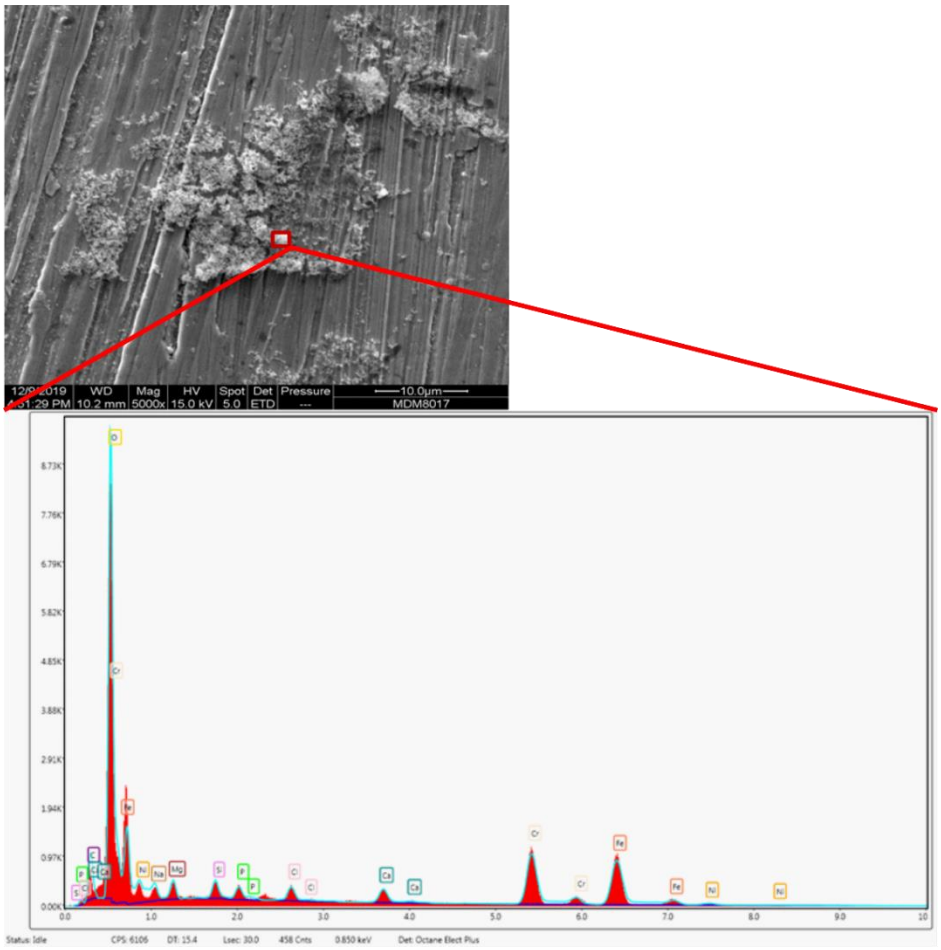

Figure 16. SEM image and EDX point analysis spectrum from experiment MDM817

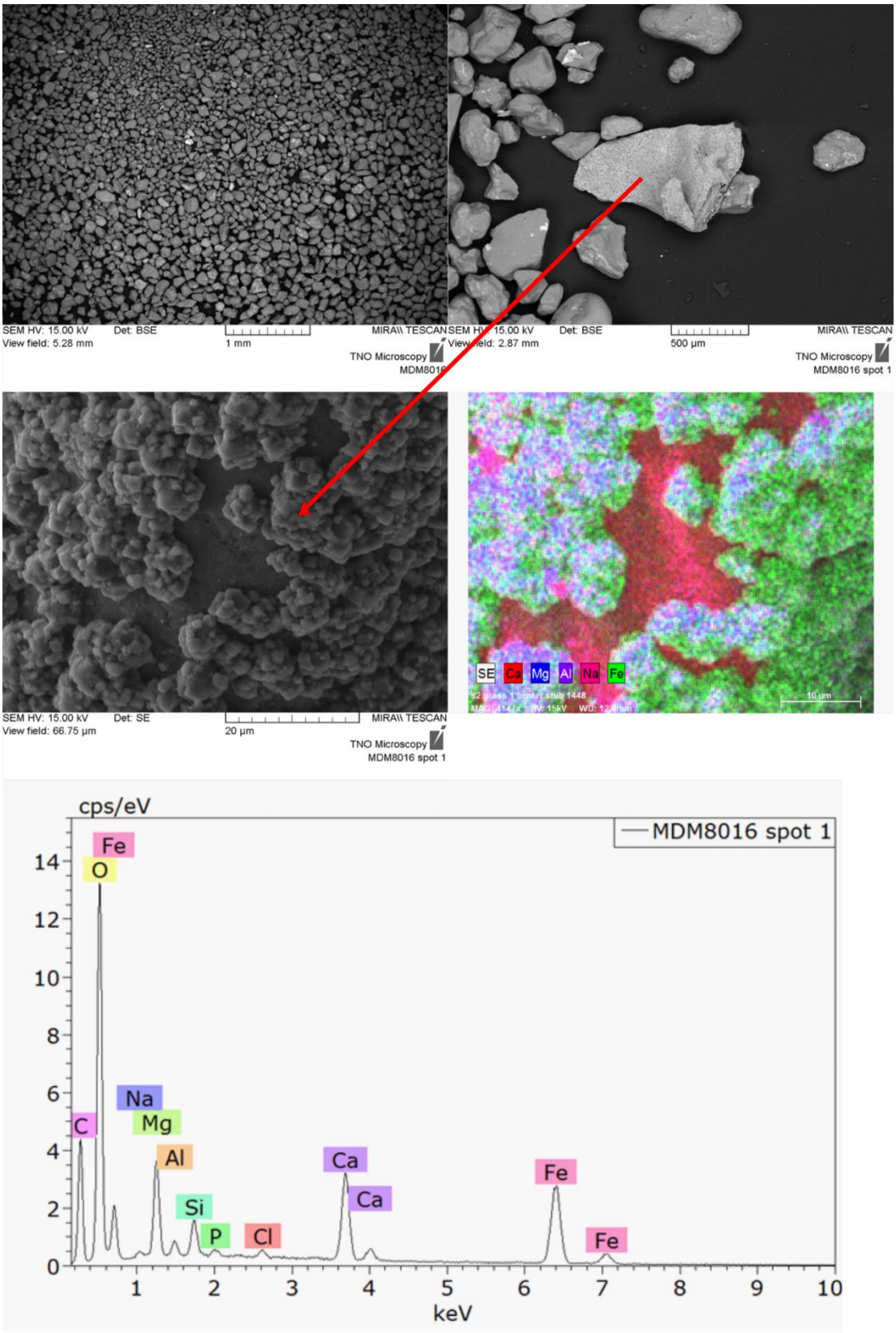

Figure 17. SEM/EDX from sediment sample from experiment MDM816. Top left: overview of sediment sample, top right: shell fragment. Middle and bottom images EDX mapping and spectrum zoomed in on shells surface.

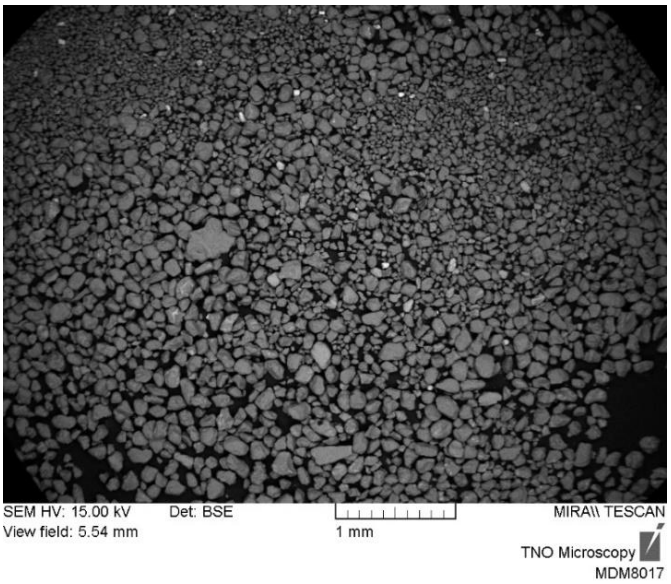

Figure 18. Overview of sediment sample from experiment MDM817

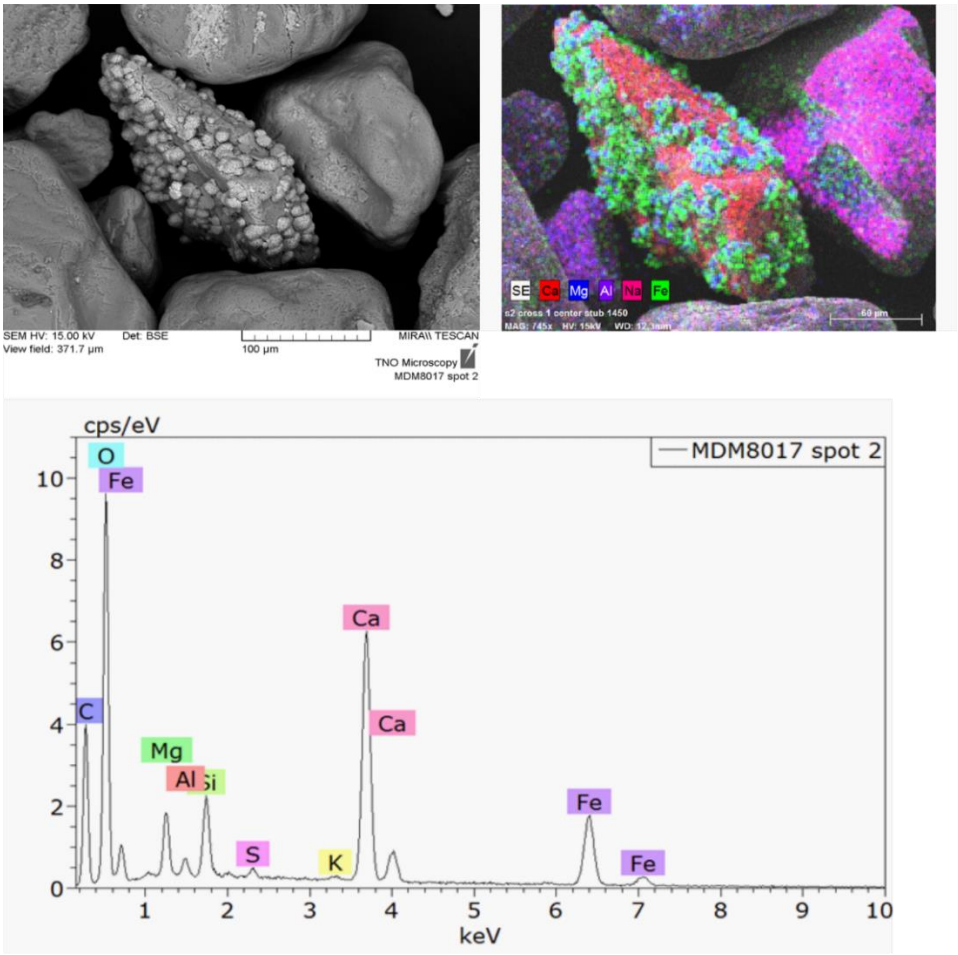

Figure 19. SEM/EDX mapping and spectrum on shell fragment from sediment sample from experiment MDM817.

4.3 Discussion of experimental results

The experiments in which the groundwater was heated in the presence of a stainless steel plate do not show signs of mineral precipitates. Some amorphous material containing all potential elements is considered to be the result of evaporation of a remaining groundwater droplet at the end of the experiment.
The experiment with calcite crystal seeds added to the autoclave resulted in the cementation of the crystals, and the crystals were on average larger than the crystals at the start of the experiment. Small crystals were found which were identified as Ca-Mg carbonates and which have most probably precipitated during the experiment.
The two water analyses for this experiment were the only two that showed a lower Ca concentration, even though the decrease was insignificant for one of the samples. In addition, the aqueous speciation modelling demonstrated that this was the only experiment for which the SI for calcite and dolomite was lower after heating than for the initial groundwater. Overall, even though more experiments and analyses are needed to support this, the results suggest that in the presence of calcite crystals, the precipitation of Ca-Mg and/or Ca carbonates is enhanced. It is generally acknowledged that the availability of a crystal surface as a seed for precipitation is kinetically favoured over homogeneous nucleation from a fluid in the absence of a proper seed for precipitation.
The experiments performed in the presence of sediment material do not show evidence for carbonate precipitation. The sediment itself contains too many different mineral phases to see changes with the SEM before and after heating. Also the water analyses and speciation modelling do not support the potential precipitation of carbonate minerals during the experiment. The presence of natural inhibitors, which are absent in the experiment with the calcite crystals, might have prevented carbonate precipitation.

5 Reactive transport modelling

5.1 Introduction

The experimental study gave a first indication that Ca-Mg carbonate precipitation, related to oversaturation as a result of heating, might occur in the aquifer where nucleation sites are present in the form of calcite crystal seeds, rather than in the heat exchanger, pipeline or injection well. In a HT-ATES system, massive amounts of heated groundwater, will be injected into the reservoir during the loading phase. The groundwater, which is generally saturated with calcite and potentially other carbonate minerals, may become oversaturated upon heating, implying that the near-well area of the aquifer may experience flow of massive amounts of groundwater which is oversaturated with these carbonates. Batch and reactive transport simulations were performed to assess the thermodynamic scaling potential and the lateral spreading of potential scaling, and its impact on the injectivity. In a next step, the efficiency of water treatment by CO_2 addition was investigated.

5.2 Model set-up

A reactive transport model, based on the planned HT-ATES system in Middenmeer, was developed using the TOUGHREACT software version 3.32 (Xu et al., 2017). The model consists of 10 layers, the upper and lower layers represent the over- and underburden with thicknesses of respectively 80 and 45 m. The 8 aquifer layers in between are each 2.25 m thick so 18 m in total. The mesh is 600 x 545 m in horizontal direction, with the 'hot well' (injector during loading and producer during unloading) and 'cold well' (producer during loading and injector during unloading) 195 m apart. The 10 cells adjacent to the wells are each 5 x 5 meter. Farther away, the sizes of the cells increase to 10 and 20 m with outer cells being 100 x 20 m to create sufficient volume for pressure dissipation. The initial groundwater temperature is 21°C, the average pressure is 35 bar. The initial aquifer porosity and horizontal and vertical permeability are 0.15 and $1.26 \cdot 10^{-11}$ m^2 and $3.16 \cdot 10^{-12}$ m^2, respectively. In the reactive transport simulations the minerals reactions are kinetically controlled. Reaction kinetics in TOUGHREACT are based on the rate expression by Lasaga et al. (1994):

$$r_n = f(c_1, c_2, ..., c_{N_C}) = \pm k_n A_n \left| 1 - \Omega_n^{\theta} \right|^{\eta}$$

Where a positive value indicates dissolution and negative value precipitation, k_n is the rate constant, A_n the specific reactive surface area and Ω_n the kinetic mineral saturation ratio. The parameters θ and η are generally determined experimentally for different minerals.
The reaction rate constant k is temperature dependent using the Arrhenius equation (Xu et al., 2004):

$$k = k_{25}^{nu} \exp\left[\frac{-E_a^{nu}}{R}\left(\frac{1}{T} - \frac{1}{298.15}\right)\right] + k_{25}^{H} \exp\left[\frac{-E_a^{H}}{R}\left(\frac{1}{T} - \frac{1}{298.15}\right)\right] a_H^{n_H} + k_{25}^{OH} \exp\left[\frac{-E_a^{OH}}{R}\left(\frac{1}{T} - \frac{1}{298.15}\right)\right] a_{OH}^{n_{OH}}$$

Where superscripts/subscripts *nu*, *H* and *OH* indicate neutral, acid and base mechanisms respectively, a is the activity of the species and n is a power term. A porosity-permeability relation is included based on the Verma and Pruess equation (1988), with a critical porosity of 10% and a power law component of 2. The kinetic parameters used in the model are shown in Table 13.
Note that for precipitation the neutral mechanisms are used, with an initial volume fraction ($V_{mineral}/V_{solid}$) assumed for calculating the initial effective surface area of 1.0E-06.

The loading/unloading scheme for the Middenmeer HT-ATES system is shown in Table 11. The unloading phase is subdivided into two sub-phases, based on the heat demand by the greenhouses during the winter months. At the end of the unloading phase, one month of 'rest' is foreseen in which no activities take place.
For the initial groundwater composition, an average composition of the measured baseline water samples was used. The rock mineralogy is represented by a simplified mineral composition (Table 12) based on an average rock mineralogy as measured by XRD (Table 10).

Table 11. Loading and unloading scheme as foreseen for the HT-ATES system in Middenmeer.

Phase	**Duration**	**Flow rate**	**T hot/cold wells**
Loading	4 months	150 m^3/hr	85°C/21°C*
Unloading			
Sub-phase 1	3 months	30 m^3/hr	85°C*/35°C
Sub-phase 2	4 months	100 m^3/hr	85°C*/35°C
Rest	1 month	-	-

*These temperatures will vary. During the loading phase the water at the cold well will initially be 21°C, whereas it will be at least 35°C in the second and next loading phases. The unloading temperature at the hot well will start at 85°C but will decrease with time.

Table 12. Simplified mineralogy used in the simulations. The minerals initially present are allowed to dissolve or precipitate, depending on the saturation index. The minerals included as secondary minerals are allowed to precipitate if the saturation index exceeds zero.

Mineral	**Rock volume fraction**
Quartz	0.889
K-feldspar	0.071
Calcite	0.018
Dolomite	0.002
Pyrite	0.001
Smectite	0.014
Kaolinite	0.005
Anhydrite	Secondary mineral
Siderite	Secondary mineral
Magnesite	Secondary mineral

Table 13. Parameters describing the kinetics of mineral reactions at 25°C: dissolution rate constant (k_{25} in mol/m^{2}s), activation energy (E_a in kJ/mol), and reaction order parameter (n). Parameters are taken from Palandri and Kharaka (2004). Mineral surface area (A_{ms}) are in cm^2/g.

	Acid mechanism			**Neutral mechanism**		**Base/carbonate mechanism**			
Mineral	**k_{25}**	**E_a**	**n**	**k_{25}**	**E_a**	**k_{25}**	**E_a**	**n**	**A_{ms}**
Quartz	-	-	-	1.02E-14	87.6	-	-	-	9.8
K-Feldspar	8.71E-11	51.7	0.5	3.89E-13	38	6.31E-22	94.1	-0.82	9.8
Calcite	5.01E-01	14.4	1.0	1.55E-06	23.5	-	-	-	9.8
Dolomite	6.46E-04	36.1	1.0	2.95E-08	52.2	7.76E-06	34.8	1.0	9.8
Pyrite	3.02E-05	56.9	1.0	2.82E-05	56.9	-	-	-	9.8
Smectite	1.05E-11	23.6	0.34	1.66E-13	35.0	3.02E-17	58.9	-0.4	151.6
Kaolinite	4.90E-12	65.9	0.78	6.61E-14	22.2	8.91E-18	17.9	-0.47	151.6
Anhydrite	-	-	-	6.46E-04	14.3	-	-	-	9.8
Siderite	6.46E-04	36.1	1.0	2.95E-08	52.2	7.76E-06	34.8	1.0	9.8
Magnesite	4.17E-07	14.4	1.0	4.57E-10	23.5	6.03E-06	62.8	1.0	9.8

Initially, the formation water composition is the same throughout the reservoir, assuming a homogeneous reservoir composition. After the first loading phase, the composition will change as a result of mineral reactions which occur primarily around the hot well, and the composition will vary in between the hot and cold wells. Unfortunately, the software does not allow the coupling of the injected water composition with the production water and hence a constant composition has to be chosen for each simulated phase relevant for the extracted groundwater during each phase.

5.3 Model results

5.3.1 Batch equilibrium simulations

In a first step, the initial formation water composition was heated in a batch equilibrium simulation to 85°C to assess the scaling potential. The batch simulation was performed with a single aquifer grid cell. For a scenario in which calcite is the only mineral which is allowed to react, small amounts of calcite are predicted to precipitate due to the oversaturation upon heating of the water to 85°C. However, when the full (simplified) mineralogy is considered, calcite is predicted to dissolve, and instead dolomite is predicted to precipitate. The precipitation of dolomite is predicted to be dominant, forcing calcite to dissolve and provide calcium for dolomite by the following reactions:

$CaCO_3 + H^+ \leftrightarrow Ca^{2+} + HCO_3^-$
$Ca^{2+} + Mg^{2+} + 2HCO_3^- \leftrightarrow CaMg(CO_3)_2$

Siderite is not predicted to precipitate and no other mineral reactions are predicted to occur. Note that the heating for this scenario was performed in several steps to prevent convergence issues. Figure 20 shows the simulated changes in rock volume fraction related to dolomite and calcite reactions for the two scenarios. In both scenarios the net porosity change is negligible.

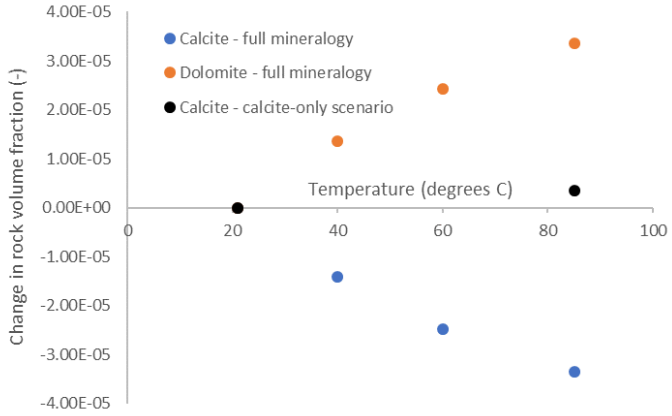

Figure 20. Simulated changes in rock volume fraction related to dolomite and calcite reactions for a scenario with the full (simplified) mineralogy and for a scenario in which only calcite is allowed to react.

Note that it is uncertain whether dolomite precipitation is possible under the conditions of this HT-ATES system. From thermodynamic and kinetic point of view, the model predicts dolomite precipitation. No direct evidence from experimental or field studies is available in literature for the precipitation of dolomite. The reactive transport simulations are performed for two scenarios: 1) no inhibition of dolomite; and 2) complete inhibition of dolomite. In the second scenario only calcite is allowed to dissolve or precipitate.

5.3.2 Reactive transport simulations

Cold water is withdrawn from one well and hot water is injected at the other well during loading. Initially, the composition of the injected water is the same as the ambient groundwater, but injected at a temperature of 85°C. During unloading, hot water is withdrawn from the hot well, the water is re-injected into the cold well at a temperature of 35°C. Figure 21 shows the simulated temperature profiles after loading and unloading, Figure 22 shows the temperature evolution at the cold well during loading and at the hot well during unloading. During loading, the hot temperature front progresses into the aquifer. The temperature at the cold well starts to increase after approximately 2 months with a final temperature of ~49°C at the end of the first loading phase. During unloading, the hot front retreats towards the hot well. At the end of the first unloading phase, the temperature at the hot well is 53°C. During the second loading phase the starting temperature at the cold well is higher due to the injection temperature of 35°C during unloading. The final temperature at the cold well at the end of the loading phase is 54°C. The temperature drop at the hot well is lower during the second unloading phase with a final temperature of 61°C.

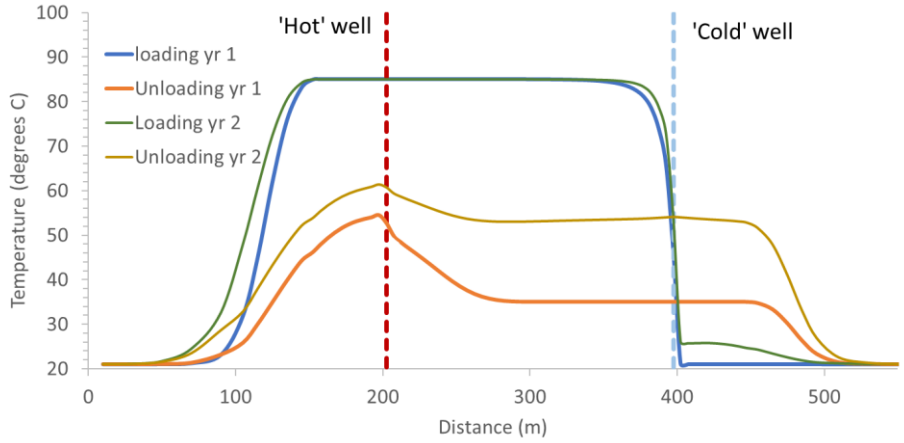

Figure 21. Temperature profiles at a depth of ~8 m below top of the aquifer, after loading and unloading for the first 2 years for scenario 1. The profiles are similar for scenario 2.

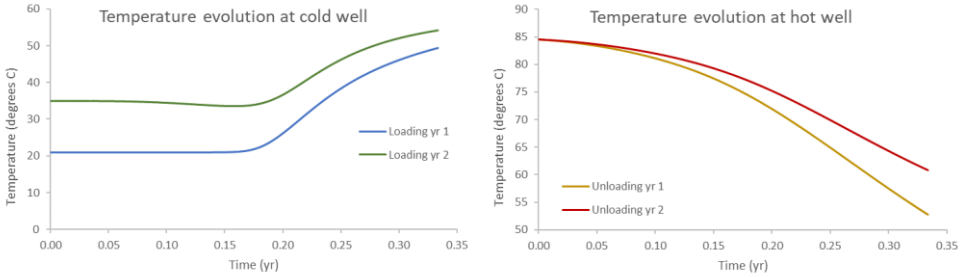

Figure 22. Temperature evolution at the cold well during loading (left) and at the hot well during unloading (right) at a depth of ~8 m below top of the aquifer for scenario 1. The profiles are similar for scenario 2. Note that for the unloading phase, only the last four months at high flow rate are shown. The temperature axis is different for the two graphs.

<u>Impact of loading on the 'hot' well</u>

The increase in temperature around the injection well changes the chemical equilibrium of the system locally. For scenario 1, dolomite starts to precipitate, extracting Mg and Ca from the groundwater. The decrease in Ca concentration causes calcite to dissolve, thereby releasing more Ca available for dolomite precipitation, as was also shown in the batch simulation. In addition, the porosity goes down from 15% to 13.8% in the area close to the well at the end of the 3 months of loading (Figure 23). Depending on the porosity-permeability relation used in the model, the permeability goes down. With the applied relation, the permeability reduces to $1.8 \cdot 10^{-12}$ m^2. Away from the well, the reactions are less advanced. For the scenario 2, calcite is predicted to precipitate around the hot well, with a very similar effect on porosity and permeability as for the full mineralogy scenario (Figure 23). The mineral reactions are most pronounced around the hot well, but they have progressed approximately 50 m into the reservoir (Figure 23).

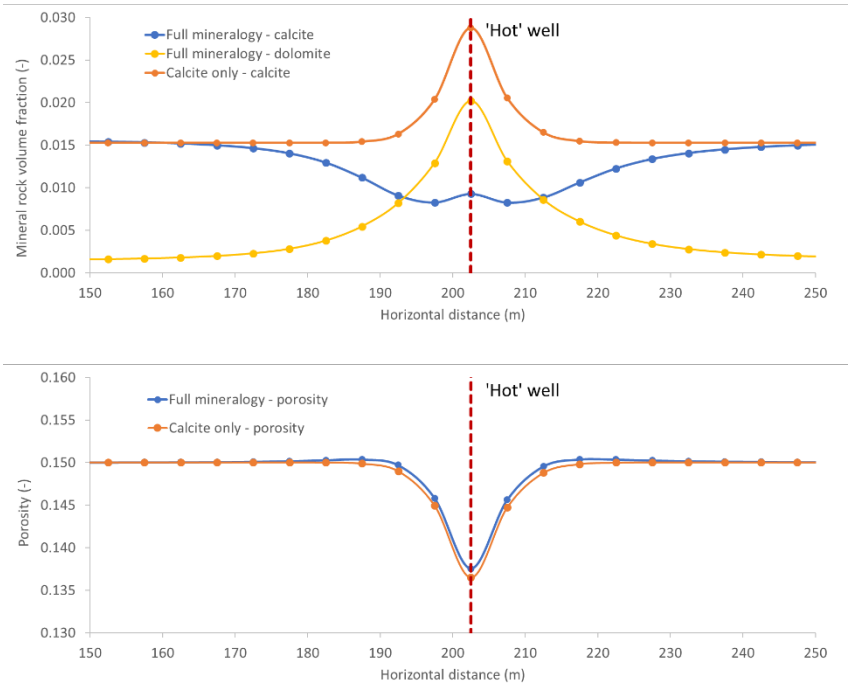

Figure 23. Simulation results for calcite and dolomite volume fraction (upper graph) and porosity (lower graph) around the hot well (red dotted line at a horizontal distance of 202.5m) after the first loading phase for scenario 1 (full mineralogy) and scenario 2 (calcite only).

Impact of unloading on the 'cold' well

At the cold well the temperature is ~50°C at the start of the unloading phase. The water withdrawn from the hot well, initially at a temperature of 85°C and decreasing with time, is cooled to 35°C and injected at the cold well. The water is in near-equilibrium with calcite and dolomite at high temperature; both minerals are slightly oversaturated due to kinetics. This near-equilibrium changes when the water is cooled and the groundwater becomes undersaturated for both minerals. For scenario 1, both dolomite and calcite are predicted to dissolve (Figure 24). The initial amount of dolomite present in the reservoir is very low and the near well zone becomes depleted in dolomite quickly. For scenario 2 only calcite is allowed to dissolve. The amount of calcite dissolution is slightly higher than for scenario 1 (Figure 24). The near-well porosity increase related to the dissolution reactions is slightly higher for scenario 2 (Figure 24). At the hot well, hardly any new changes are predicted to occur during unloading.

With subsequent loading and unloading phases, these trends described for the mineral reactions and corresponding porosity changes around the hot and cold wells continue. The effects around the wells become more advanced, and they progress further into the aquifer. Figure 25 shows the simulated permeability profiles after the first and second unloading phases. Note that the permeability change is highly dependent on the model input parameters. The key message from the results is the tendency of porosity and permeability decrease around the hot well and increase around the cold well.

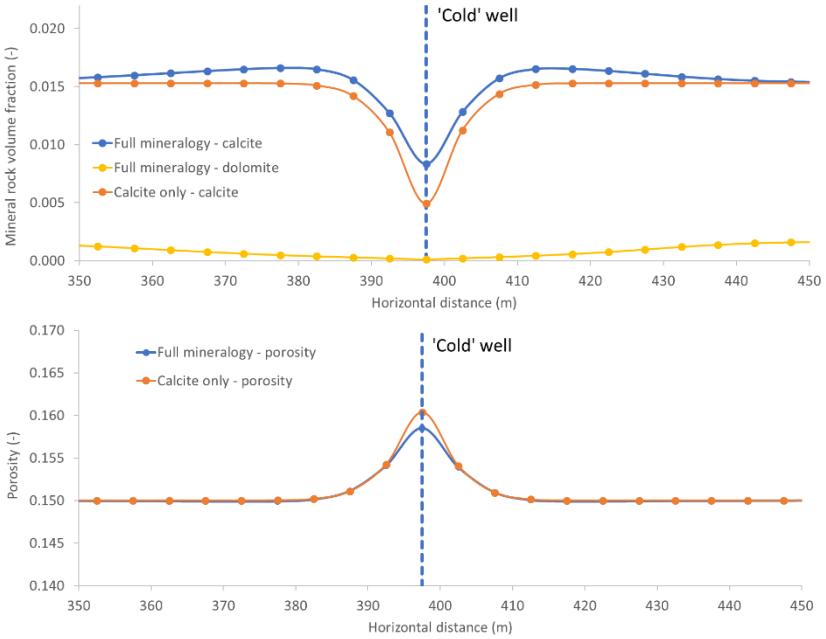

Figure 24. Simulation results for calcite and dolomite fraction (upper graph) and porosity (lower graph) around the cold well (blue dotted line at a horizontal distance of 397.5m) after the first unloading phase for scenario 1 (full mineralogy) and scenario 2 (calcite only).

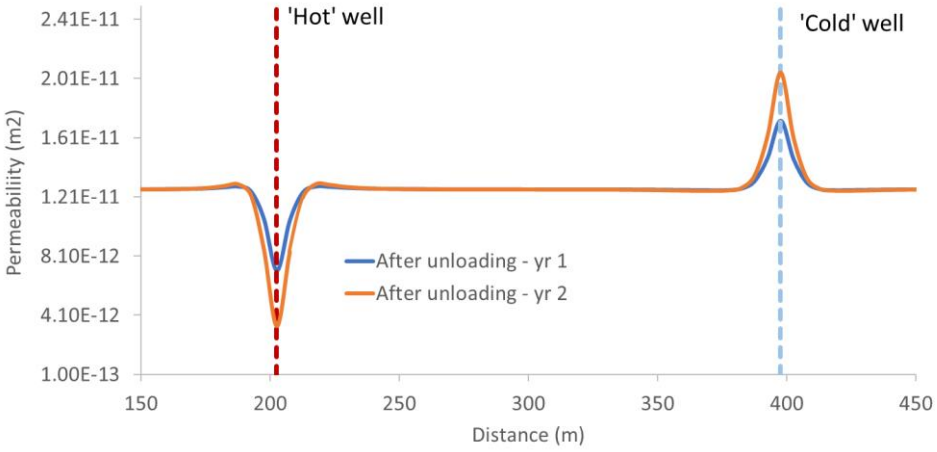

Figure 25. Permeability profiles after the first and second unloading phases for scenario 1.

Water treatment by CO_2

The addition of CO_2 to the injected water is recognized as treatment procedure to prevent carbonate scaling at the hot well. PHREEQC simulations performed by IF Technology (Schrijver (2020), personal communication) resulted in the required addition of 1.49 mmol CO_2/l (0.06 g/kg water) for the first loading phase to keep the saturation index of calcite at zero. This amount of CO_2 is co-injected at the hot well in the simulation to assess the impact of this water treatment. The TOUGHREACT results show that this amount is more than enough to prevent scaling. In fact, the porosity around the injection well increases in the first year of loading due to a (net) dissolution effect with corresponding porosity increase for both scenarios (Figure 26). For scenario 1, dolomite precipitation still occurs but is much lower than for the base

case, and calcite dissolution is enhanced compared to the base case. In year 2, the porosity increase from the first loading phase is nullified due to the depletion of calcite around the well and continuation of minor dolomite precipitation. For scenario 2, calcite dissolution is also predicted to occur.
During the unloading phase the water has a much higher dissolved CO_2 content and lower pH than in the base cases (scenario 1 and 2 without water treatment). As a result, both dolomite and calcite solubility in scenario 1 and calcite solubility in scenario 2, is enhanced around the cold well and the porosity increase is enhanced compared to the base case scenario. Lower amounts of CO_2 addition might suffice against scaling. Calculation of the exact amount is outside the scope of this study.

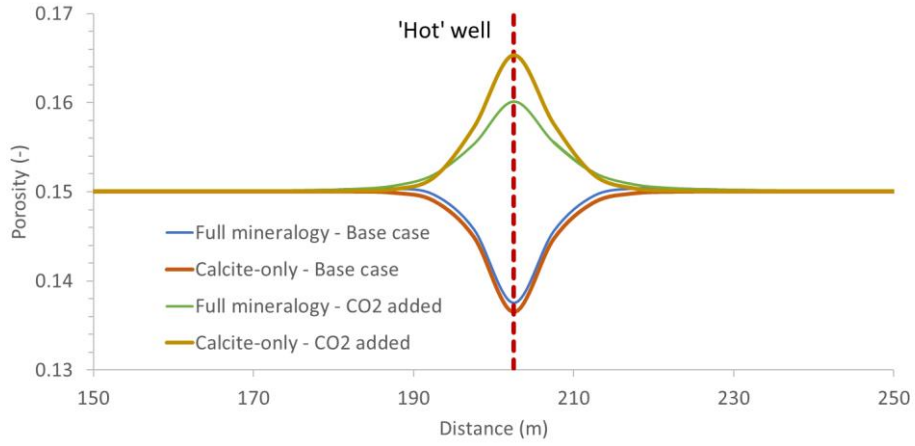

Figure 26. Simulation results for porosity after the first loading phase, for the base cases and the scenarios with CO_2 added as mitigation for scaling (1.49 mmol/l water).

5.4 Implications for HT-ATES in Middenmeer

The temperature changes upon loading and unloading in a HT-ATES system will induce geochemical reactions. The simulations predict carbonate scaling to occur around the hot well and dissolution around the cold well. With each next cycle, the mineral reactions continue. As a consequence, the porosity and permeability around the hot well would go down. It should be noted that the exact extent of the mineral reactions and corresponding porosity and permeability changes are uncertain and the model results should be interpreted with care as no full account of the kinetics of the carbonate mineral reactions could be made. Yet, the trends of scale formation around the hot well and dissolution around the cold well should be considered in the design and operations of the site as scale formation around the hot well would increase the risk of injectivity/productivity problems. On the other hand, an increased porosity around the cold well could enhance the flow properties, but they could also induce geomechanical effects, such as pore collapse. The assessment of such a geomechanical risk is outside the scope of this report.
The model results show that the addition of CO_2 to the injected water during loading phases can be efficient against carbonate scaling around the hot well. The applied dosing of CO_2 seems to be on the high side since a significant porosity increase is predicted to occur around the hot well due to carbonate dissolution. A lower dosing might be sufficient to prevent either scaling or dissolution. The downside of the water

treatment with CO_2, even if the dosing would be adjusted to prevent a porosity change around the hot well, is the enhanced porosity increase around the cold well during the unloading phase, related to the higher concentration of dissolved CO_2 in the cooled water and the lower pH. The geomechanical effects should be investigated. The removal of CO_2 from the withdrawn water prior to injection into the cold well during the unloading phase should be considered.

6 Discussion and conclusions

The aim of this project was to develop a workflow for the determination of the risk of scaling in a HT-ATES system by application to the potential site at Agriport in Middenmeer, The Netherlands. A methodology for water sampling on a site, thereby keeping the sampled water at pressure, and transferring the water to an experimental, oxygen-free autoclave was successfully developed and applied. A series of experiments were performed using groundwater from the site, with or without the addition of calcite crystals or aquifer sediment. A small steel plate was added to the autoclave for each experiment to represent the stainless steel components of the engineered parts of the system.

The experiments demonstrated that, even though the groundwater will become supersaturated with carbonates upon heating, precipitation of the carbonates does not occur in the absence of calcite or aquifer sediment, representative for conditions in the engineered part of the system (pipes and well). The experiments represented batch conditions, whereas the water in the HT-ATES system would be in constant flow conditions. Depending on the flow rate, the water will be withdrawn from one well and injected in the next well within a time frame of 15 minutes to 2 hours. Hence, the residence time of the water in the engineered system is already much lower than the duration of the experiments performed in this study. In addition, flow conditions may lower the scaling potential for carbonates in the pipes and well compared to batch conditions as flow conditions may induce small precipitates to be dragged along with the water as suspension. Therefore, the batch reaction experiments already provide more stringent conditions than can be expected in the real system. Yet, in the absence of minerals as growth sites, with only a steel plate present to represent the stainless steel components of the engineered system, no precipitation seems to have taken place.

In the presence of the calcite seeds, the initially separate calcite crystals have been partially cemented and the crystals are larger than at the start of the experiment. Ca and/or Ca-Mg carbonate precipitation and/or recrystallization seems to have taken place. The water analyses performed prior to and after the experiment support the observed precipitation of calcite, as these are the only experiments for which a decrease in calcium concentration in the water was measured. Although small carbonate crystals were found that contained both Ca and Mg, and the crystals most probably precipitated during the experiment, a decrease in Mg concentration in the water was not measured. It should be noted that the changes in Ca and Mg concentrations are minor, and the water analyses are prone to analytical variability as the samples were analysed in different batches. It is thus hard to separate differences in concentration due to a hydrochemical process among the different experiments from differences due to analytical error. Aqueous speciation modelling demonstrated supersaturation for both calcite and dolomite, supporting the potential precipitation of these minerals in near-well environments. Anyhow, the small differences indicate that no large amounts of carbonate (and other minerals) become precipitated from these small volumes of groundwater. The presence of a small steel plate also plays a role as steel corrosion was found to be relevant at least with respect to the water composition. For this reason, the theory that calcite crystals will act as growth sites for calcite, and hence, carbonate scaling is more likely in the calcareous reservoir during injection of hot water than in the technical installation requires

additional experiments and perhaps a change in the methodology for water composition analysis. For the experiments performed with aquifer sediment, any changes in the mineralogy were difficult to observe. The water composition analyses do not support the potential precipitation of calcite, dolomite or other carbonate minerals. The Maassluis aquifer sediment which was added to the autoclave is composed of coastal marine sands which consist mainly of quartz. Minor percentages of calcite (~ 2%) in the form of shells and forams were observed by the microscope. Possibly, pure calcite crystals are more prone to promoting precipitation of calcite than forams, which would explain the difference in experimental results between the experiments with calcite seeds and aquifer sediment. The shells in the sediment are all covered with an iron-rich carbonates, presumably siderite. In addition, the presence of organic carbon could have prevented carbonate precipitation.

Overall, the experiments suggest that the risk of scaling by Ca-Mg carbonates for the potential site at Middenmeer is higher in the aquifer where crystal growth sites are present, than in the technical part of the HT-ATES system, although more experiments are required to confirm this. The reactive transport model, simulating inorganic chemical reactions in the aquifer during loading and unloading phases, predict that, instead of calcite scaling, dolomite scaling is thermodynamically favoured in the reservoir around the hot well during the loading phase. Calcite is in fact 'forced' to dissolve to provide the calcium required for dolomite precipitation. Around the cold well, both calcite and dolomite are predicted to dissolve during the unloading phase. The net result is basically a re-distribution of carbonate minerals from the cold zone to the hot zone, with calcite providing additional Ca. As a result of the mineral reactions, the porosity and permeability may decrease around the hot well during loading and increase around the cold well during unloading. With each next cycle, the reactions continue and progress further into the aquifer. The exact impact is hard to foresee as model simplifications and uncertainties will impact the kinetics of carbonate reactions and thus the extent of the area vulnerable for changes in porosity and hence permeability.

It should be noted that the results should be interpreted with care. The model simulates inorganic mineral dissolution and precipitation reactions based on thermodynamic and kinetic considerations, but minerals reactions can be affected by processes currently not included in the simulations. These include, among others, inhibition by the presence of natural inhibitors, impact of organic material and cation exchange reactions. To the best of our knowledge, besides the EDX analysis performed on one precipitate in our experiment demonstrating the presence of Mg in the Ca carbonate, no direct evidence for dolomite scaling in HT-ATES systems has been reported and the precipitation of dolomite could be subject to inhibition. Bonte et al. (2013) performed flow experiments through sandstone cores and linked a Mg decrease in the water at an experimental temperature of 60°C to dolomite precipitation. Jesußek et al. (2013) oppositely, also observed a Mg decrease in their experiments but excluded the possibility of dolomite precipitation due to the absence of a concurrent decrease in total inorganic carbon. Dolomite precipitation might be inhibited by several different mechanisms, but a review of such mechanisms is outside the scope of this study. An alternative model, allowing the dissolution and precipitation of calcite only, resulted in calcite deposition near the hot well and dissolution near the cold well. The associated porosity changes are very similar to those predicted for the base case. The lateral spreading of carbonate dissolution and precipitation as simulated by the model is subject to the model set-up and chosen

input parameters. Yet, the overall trend of carbonate precipitation with corresponding porosity and permeability decrease around the hot well, and carbonate dissolution with corresponding porosity and permeability increase around the cold well should be considered in the operational design of the site. Monitoring data will be highly valuable in the validation and calibration of the model.

The addition of CO_2 to the water prior to injection into the hot well during loading can be an effective means to prevent the scaling by carbonates. The amount of CO_2 should be carefully defined using geochemical modelling in order to prevent significant dissolution of all carbonate minerals present with corresponding porosity and permeability increases. In addition, it will significantly enhance the dissolution process around the cold well, unless the CO_2 is removed from the groundwater prior to injection during the unloading phase. Minor porosity and permeability increase can be beneficial for the injectivity and productivity. Oppositely, major increases could have a negative geomechanical impact such as pore collapse.

Naturally, these experimental and numerical modelling results are specific for the reservoir water composition and experimental/modelling conditions used in this study. Mineral scaling, primarily by calcite, has been observed in the engineered system of operational HT-ATES systems, for example in the heat exchanger or the pipes (Knoche et al., 2003). According to experiments performed by Knoche et al. (2003) the salinity of the water plays an important role, with higher salinities resulting in lower scaling risk. For every potential HT-ATES system, the risk of scaling and the location in the system at which the scaling potential is largest should be assessed. Uncertainties in the geochemical response of a system to heating, which are difficult to address in experimental or numerical studies remain. A workflow with experimental and numerical model approach such as presented in this study can be applied for a specific site as a first evaluation of the risk, nature and location of scaling. During operations of a HT-ATES system, it is recommended to perform careful monitoring, calibrate the numerical model(s), and adapt the operational design if necessary.

7 References

Bonte, M., Van Breukelen, B. M., & Stuyfzand, P. J. (2013). Environmental impacts of aquifer thermal energy storage investigated by field and laboratory experiments. *Journal of Water and Climate Change*, *4*(2), 77-89. doi:10.2166/wcc.2013.061

Brons, H., Griffioen, J., Appelo, C., & Zehnder, A. (1991). (Bio)geochemical reactions in aquifer material from a thermal energy storage site. *Water Research*, *25*(6), 729-736. doi:10.1016/0043-1354(91)90048-u

De Jonge, H. (2017). *Hoge temperatuuropslag in Agriport in Middenmeer*. IF Technology bv.

Dinkelman, D. (2019). Optimization of technical and economic efficiency of HT-ATES combined with geothermal energy – Case study modelling of Agriport A7, Middenmeer. Msc thesis, Utrecht University.

Ebbing, J.H.J & De Lang, F.D. (2003). *Formatie van Oosterhout.* TNO-NITG. Lithostratigrafische nomenclator ondiepe ondergrond Nederland.

Griffioen, J., & Appelo, C.A.J. (1993). Nature and extent of carbonate precipitation during aquifer thermal energy storage. Applied Geochemistry 8(2), 161-176.

Huizer, J., & Weerts, H. (2003). *Beschrijving lithostratigrafische eenheid: de Formatie van Maassluis*. TNO.

IF Technology. (2019). *Hoge Temperatuur Opslag, ECW Agriport Middenmeer – Rapportage uitvoering proefboring MDM-HTO-01. IF report 67196/BP/20190712*.

Jesußek, A., Grandel, S. & Dahmke, A. (2013). Impacts of subsurface heat storage on aquifer hydrogeochemistry. Enivronmental Earth Sciences 69, 1999-2012. DOI 10.1007/s12665-012-2037-9.

Knoche, G., Koch, M. & Metzger J.W. (2003). Scaling-tests on groundwater for use in High-Temperature-ATES in respect to calcite precipitates in heat exchangers. 9th international conference on thermal energy storage, Warsaw, Poland.

Lasaga, A.C., Soler, J.M., Ganor J., Burch, T.E.,& Nagy, K.L.(1994). Chemical weathering rate laws and global geochemical cycles. Geochimica et. Cosmochimica Acta v.58, p2361-2386.

Xu, T., Sonnenthal, E., Spycher, N. & Zheng, L. (2017). TOUGHREACT V3.32 Reference manual: A parallel simulation program for non-isothermal multiphase geochemical reactive transport. LBNL-DRAFT.

Appendix

In this Appendix, 5 tables with water compositions from the experiments are presented and include:

Table 14. Measured water compositions for Experiment 1. MDM500 and MDM800 are water batches from the experiments prior to heating, MDM 501 and MDM801 are their respective batches after heating.

Table 15. Measured water compositions for Experiment 2. MDM001 is the water batch from the experiment prior to heating, MDM802 and MDM803 are the batches after heating.

Table 16. Measured water compositions for Experiment 3. MDM009 is the water batch from the experiments prior to heating, MDM 809 and MDM810 are the batches after heating.

Table 17. Measured water compositions for Experiment 4. MDM012 is the water batch from the experiments prior to heating, MDM813 and MDM814 are the batches after heating.

Table 18. Measured water compositions for Experiment 5. MDM015 is the water batch from the experiments prior to heating, MDM 813 and MDM814 are the batches after heating.

Table 14. Measured water compositions for Experiment 1. MDM500 and MDM800 are water batches from the experiments prior to heating, MDM 501 and MDM801 are their respective batches after heating.

EXPERIMENT 1		**MDM500 - 18-09-2019**	**MDM501 - 19-09-2019**	**MDM801- 19-09-2019**	**Δ MDM501-500**	**Δ MDM801-500**
Element	***Unit***	***0 days***	***1 day***	***1 day***	***%***	***%***
Doc	mg/L	6.170	13.260	10.780	114.9	74.7
Chloride	mg/L	10697.195	10780.821	10684.915	0.8	-0.1
Nitrate	mg/L	0.000	0.000	0.000	0.0	0.0
Sulphate	mg/L	0.000	3.571	0.000	100.0	0.0
Nitrate	mg/L	0.000	0.000	0.000	0.0	0.0
Aluminium	mg/L	0.038	0.022	0.129	-41.7	240.2
Arsenic	mg/L	0.000	0.001	0.001	5499.8	6142.8
Barium	mg/L	0.171	0.715	0.734	318.1	328.9
Calcium	mg/L	428.250	430.500	429.800	0.5	0.4
Cadmium	mg/L	0.000	0.000	0.000	-80.3	-59.2
Chrome	mg/L	0.001	0.001	0.002	31.8	125.6
Copper	mg/L	0.032	0.050	0.086	58.6	171.4
Iron	mg/L	1.137	0.022	0.038	-98.1	-96.6
Potassium	mg/L	98.925	93.870	93.800	-5.1	-5.2
Magnesium	mg/L	543.750	518.600	514.300	-4.6	-5.4
Manganese	mg/L	0.221	0.215	0.192	-2.9	-13.4
Sodium	mg/L	5694.000	5408.000	5409.000	-5.0	-5.0
Nickel	mg/L	0.008	0.053	0.032	560.3	295.5
Total phosphorus	mg/L	0.888	0.393	0.410	-55.8	-53.9
Led	mg/L	0.004	0.001	0.002	-73.0	-53.6
Strontium	mg/L	18.398	17.965	18.815	-2.4	2.3
Zinc	mg/L	0.135	0.088	0.117	-35.0	-13.6
Ammonium	mg/L	72.031	75.389	74.965	4.7	4.1
Phosphate	mg/L	1.911	0.921	1.111	-51.8	-41.9
Lithium	mg/L	0.201	0.203	0.202	1.0	0.5
Silicon	mg/L	10.000	10.000	10.000	0.0	0.0

Table 15. Measured water compositions for Experiment 2. MDM001 is the water batch from the experiment prior to heating, MDM802 and MDM803 are the batches after heating.

EXPERIMENT 2		**MDM001**	**MDM802**	**MDM803**	**Δ MDM001-802**	**Δ MDM001-803**
Element	***Unit***	***0 days***	***5 days***	***5 days***	***%***	***%***
Doc	mg/L	8.600	32.460	19.550	277.4	127.3
Chlorine	mg/L	10767.812	10766.176	10846.010	0.0	0.7
Nitrate	mg/L	0.000	0.000	0.000	0.0	0.0
Sulphate	mg/L	2.280	5.140	4.274	125.5	87.5
Nitrate	mg/L	*bdl*	*bdl*	*bdl*	bdl	*nr*
Aluminium	mg/L	0.036	0.148	0.267	315.5	646.5
Arsenic	mg/L	0.001	0.001	0.001	-15.8	21.1
Barium	mg/L	0.188	0.373	0.379	98.6	101.9
Calcium	mg/L	402.250	413.750	425.250	2.9	5.7
Cadmium	mg/L	*bdl*	*bdl*	*bdl*	*nr*	*nr*
Chromium	mg/L	0.003	0.003	0.003	-23.1	-8.2
Copper	mg/L	0.011	0.018	0.018	72.4	68.0
Iron	mg/L	0.774	0.382	0.393	-50.6	-49.2
Potassium	mg/L	96.925	96.400	96.800	-0.5	-0.1
Magnesium	mg/L	531.500	520.500	536.250	-2.1	0.9
Manganese	mg/L	0.227	0.253	0.275	11.2	21.1
Sodium	mg/L	5780.000	5648.000	5768.000	-2.3	-0.2
Nickel	mg/L	0.011	0.218	0.038	1964.5	258.8
Total phosphorus	mg/L	0.228	0.175	0.447	-23.4	95.8
Lead	mg/L	0.001	0.002	0.005	64.6	313.0
Strontium	mg/L	18.668	18.250	18.750	-2.2	0.4
Zinc	mg/L	0.078	0.076	0.127	-2.5	62.8
Ammonium	mg/L	69.531	74.299	71.951	6.9	3.5
Phosphate	mg/L	0.914	0.848	1.346	-7.2	47.3
Lithium	mg/L	0.203	0.206	0.215	1.5	5.9
Silicon	mg/L	10.000	11.000	12.000	10.0	20.0

Table 16. Measured water compositions for Experiment 3. MDM009 is the water batch from the experiments prior to heating, MDM 809 and MDM810 are the batches after heating.

EXPERIMENT 3		**MDM009**	**MDM809**	**MDM810**	**Δ MDM009-809**	**Δ MDM009-810**
Element	***Unit***	***0 days***	***5 days***	***5 days***	***%***	***%***
Doc	mg/L	13.010	25.010	14.230	92.2	9.4
Chlorine	mg/L	10840.114	10951.310	10881.770	1.0	0.4
Nitrate	mg/L	0.000	0.000	0.000	0.0	0.0
Sulphate	mg/L	5.331	6.762	7.996	26.8	50.0
Nitrate	mg/L	*bdl*	*bdl*	*bdl*	*nr*	*nr*
Aluminium	mg/L	0.034	0.081	0.057	139.3	69.0
Arsenic	mg/L	0.001	0.001	0.001	24.2	21.5
Barium	mg/L	0.169	0.165	0.191	-1.8	13.4
Calcium	mg/L	418.500	409.000	418.250	-2.3	-0.1
Cadmium	mg/L	*bdl*	*bdl*	*bdl*	*nr*	*nr*
Chromium	mg/L	0.001	0.001	0.001	3.6	-24.9
Copper	mg/L	0.032	0.033	0.022	2.4	-31.4
Iron	mg/L	0.468	0.192	0.145	-59.0	-69.0
Potassium	mg/L	95.700	96.725	97.000	1.1	1.4
Magnesium	mg/L	516.750	524.000	527.750	1.4	2.1
Manganese	mg/L	0.235	0.184	0.192	-21.5	-18.2
Sodium	mg/L	5555.000	5655.000	5619.000	1.8	1.2
Nickel	mg/L	0.016	0.100	0.042	517.0	158.3
Total phosphorus	mg/L	71.951	71.951	71.951	0.0	0.0
Lead	mg/L	*bdl*	*bdl*	*bdl*	*nr*	*nr*
Strontium	mg/L	0.003	0.003	0.001	19.2	-57.1
Zinc	mg/L	18.545	18.698	18.745	0.8	1.1
Ammonium	mg/L	60.100	92.725	62.575	54.3	4.1
Phosphate	mg/L	1.006	0.867	0.820	-13.8	-18.5
Lithium	mg/L	0.209	0.213	0.212	1.9	1.4
Silicon	mg/L	11.000	14.000	13.000	27.3	18.2

Table 17. Measured water compositions for Experiment 4. MDM012 is the water batch from the experiments prior to heating, MDM813 and MDM814 are the batches after heating.

EXPERIMENT 4		**MDM012**	**MDM813**	**MDM814**	**Δ MDM012-813**	**Δ MDM012-814**
Element	***Unit***	***0 days***	***5 days***	***5 days***	***%***	***%***
Doc	mg/L	6.200	11.870	9.760	91.5	57.4
Chlorine	mg/L	10848.257	10907.629	10849.125	0.5	0.0
Nitrate	mg/L	*bdl*	*bdl*	*bdl*	*nr*	*nr*
Sulphate	mg/L	*bdl*	*bdl*	*bdl*	*nr*	*nr*
Nitrate	mg/L	*bdl*	*bdl*	*bdl*	*nr*	*nr*
Aluminium	mg/L	0.022	0.082	0.064	272.7	190.9
Arsenic	mg/L	0.001	0.001	0.000	51.8	-18.8
Barium	mg/L	0.167	0.165	0.161	-1.7	-4.1
Calcium	mg/L	414.750	419.250	415.500	1.1	0.2
Cadmium	mg/L	*bdl*	*bdl*	*bdl*	*nr*	*nr*
Chromium	mg/L	0.001	0.001	0.001	16.7	45.8
Copper	mg/L	0.007	0.003	0.029	-52.2	336.1
Iron	mg/L	0.398	0.050 bdl	0.014	-87.4	-96.5
Potassium	mg/L	95.200	95.030	94.330	-0.2	-0.9
Magnesium	mg/L	512.000	520.750	514.500	1.7	0.5
Manganese	mg/L	0.214	0.211	0.210	-1.6	-1.9
Sodium	mg/L	5510.000	5529.000	5493.000	0.3	-0.3
Nickel	mg/L	0.009	0.041	0.045	348.5	392.2
Total phosphorus	mg/L	70.879	67.220	71.108	-5.2	0.3
Lead	mg/L	*bdl*	*bdl*	*bdl*	*nr*	*nr*
Strontium	mg/L	*bdl*	*bdl*	*bdl*	*nr*	*nr*
Zinc	mg/L	18.313	18.443	18.435	0.7	0.7
Ammonium	mg/L	75.700	50.800	122.100	-32.9	61.3
Phosphate	mg/L	0.912	0.942	0.922	3.3	1.1
Lithium	mg/L	0.213	0.211	0.200	-0.9	-6.1
Silicon	mg/L	11.000	15.000	13.000	36.4	18.2

Table 18. Measured water compositions for Experiment 5. MDM015 is the water batch from the experiments prior to heating, MDM 813 and MDM814 are the batches after heating

EXPERIMENT 5		**MDM015**	**MDM816**	**MDM817**	**Δ MDM015-816**	**Δ MDM012-817**
Element	***Unit***	***0 days***	***5 days***	***5 days***	***%***	***%***
Doc	mg/L	6.420	8.870	9.180	38.2	43.0
Chlorine	mg/L	10925.558	10910.122	11007.128	-0.1	0.7
Nitrate	mg/L	0.000	0.000	0.000	0.0	0.0
Sulphate	mg/L	0.000	5.489	5.047	undefined	undefined
Nitrate	mg/L	0.000	0.000	0.000	0.0	0.0
Aluminium	mg/L	*bdl*	0.035	0.062	*nr*	*nr*
Arsenic	mg/L	0.001	0.004	0.004	375.4	428.2
Barium	mg/L	0.156	0.164	0.187	5.6	20.1
Calcium	mg/L	424.250	426.250	427.000	0.5	0.6
Cadmium	mg/L	*bdl*	*bdl*	*bdl*	*nr*	*nr*
Chromium	mg/L	0.001	0.001	0.001	-20.8	-38.8
Copper	mg/L	0.003	0.031	0.013	1136.6	425.4
Iron	mg/L	0.304	0.075	1.090	-75.4	258.6
Potassium	mg/L	92.875	93.350	94.050	0.5	1.3
Magnesium	mg/L	525.500	525.000	521.000	-0.1	-0.9
Manganese	mg/L	0.212	0.170	0.188	-19.6	-11.2
Sodium	mg/L	5520.000	5500.000	5480.000	-0.4	-0.7
Nickel	mg/L	*bdl*	0.044	0.039	*nr*	*nr*
Total phosphorus	mg/L	0.326	0.313	0.269	-4.1	-17.5
Lead	mg/L	*bdl*	0.008	0.002	nr	nr
Strontium	mg/L	18.003	18.395	18.868	2.2	4.8
Zinc	mg/L	0.626	0.081	0.330	-87.0	-47.2
Ammonium	mg/L	*bdl*	*bdl*	*bdl*	*nr*	*nr*
Phosphate	mg/L	0.980	0.887	0.900	-9.5	-8.2
Lithium	mg/L	0.213	0.212	0.206	-0.5	-3.3
Silicon	mg/L	11.000	16.000	16.000	45.5	45.5